
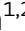









# Lipin-2 regulates the antiviral and anti-inflammatory responses to interferon

Nagore de Pablo<sup>1,†</sup> , Clara Meana<sup>1,2,†</sup> , Javier Martínez-García<sup>1,2,†</sup> , Pablo Martínez-Vicente<sup>3,4</sup> , Manuel Albert<sup>5</sup> , Susana Guerra<sup>5</sup> , Ana Angulo<sup>3,4</sup> , Jesús Balsinde<sup>1,2</sup>  & María A Balboa<sup>1,2,\*</sup> 

## Abstract

Interferons (IFN) are crucial antiviral and immunomodulatory cytokines that exert their function through the regulation of a myriad of genes, many of which are not yet characterized. Here, we reveal that lipin-2, a phosphatidic acid phosphatase whose mutations produce an autoinflammatory syndrome known as Majeed syndrome in humans, is regulated by IFN in a STAT-1-dependent manner. Lipin-2 inhibits viral replication both *in vitro* and *in vivo*. Moreover, lipin-2 also acts as a regulator of inflammation in a viral context by reducing the signaling through TLR3 and the generation of ROS and release of mtDNA that ultimately activate the NLRP3 inflammasome. Inhibitors of mtDNA release from mitochondria restrict IL-1 $\beta$  production in lipin-2-deficient animals in a model of viral infection. Finally, analyses of databases from COVID-19 patients show that *LPIN2* expression levels negatively correlate with the severity of the disease. Overall, these results uncover novel regulatory mechanisms of the IFN response driven by lipin-2 and open new perspectives for the future management of patients with *LPIN2* mutations.

**Keywords** COVID-19; inflammasome; interferon; lipin-2; MCMV

**Subject Categories** Immunology; Microbiology, Virology & Host Pathogen Interaction; Signal Transduction

**DOI** 10.15252/embr.202357238 | Received 24 March 2023 | Revised 16 October 2023 | Accepted 19 October 2023

**EMBO Reports (2023) e57238**

## Introduction

Interferons (IFNs) are essential cytokines in the fight against viral infections and also display immunomodulatory actions (Schneider *et al*, 2014). Engagement of pathogen-associated molecular patterns (PAMPs) with pattern recognition receptors (PRRs) at the plasma and endosomal membranes and the cytosol, generate IFNs (Janeway Jr & Medzhitov, 2002; Toshchakov *et al*, 2002). Once synthesized

and released from cells, they may act in an autocrine or paracrine fashion by binding to specific cell surface receptors. Although there are three categories of IFNs, only type I (IFN $\alpha$  and  $\beta$ ) and II (IFN $\gamma$ ) are relevant to immune cells. They signal through different receptors, i.e. type I IFNs bind to IFNAR, while IFN $\gamma$  binds to IFNGR. After recognition of their respective ligands, both receptors activate a signaling cascade initiated by Janus kinases (JAK), and TYK2 in the case of IFNAR, that culminates in the activation of several members of the signal transducer and activator of transcription (STAT) family, and the upregulation of interferon-stimulated genes (ISGs) (Levy *et al*, 1988; Darnell Jr *et al*, 1994). Specifically, type I IFNs promote the phosphorylation of STAT1 and STAT2 that, together with IRF9 form the interferon-stimulated gene factor 3 (ISGF3) complex. ISGF3 translocates to the nucleus and binds a DNA sequence motif known as the interferon-stimulated response element (ISREs) present in type I ISGs (Stark & Darnell Jr, 2012). On the other hand, IFN $\gamma$  promotes the phosphorylation and dimerization of STAT1, which binds to the IFN $\gamma$  activation site (GAS) DNA element to initiate the transcription of type II ISGs (Decker *et al*, 1991; Schneider *et al*, 2014). This type of ISGs can also be upregulated by type I IFNs through the promotion of STAT1 and STAT3 homo and heterodimers. ISGs participate in mounting an effective antiviral state that may help to fight intracellular bacteria and parasites, and initiate an adequate adaptive immune response (Schoggins *et al*, 2011). However, despite many years of efforts, only a few ISGs have been characterized in detail.

Lipin-2 is a member of a family of phosphatidic acid phosphatase enzymes which are central to lipid metabolism, as they provide the diacylglycerol (DAG) that is used within the *de novo* pathway for phospholipid and triacylglycerol (TAG) biosynthesis (Balboa *et al*, 1998; Péterfy *et al*, 2001; Zhang & Reue, 2017). The gene encoding for lipin-2, *LPIN2*, is mutated in patients that suffer from an autoinflammatory disease known as Majeed syndrome (Ferguson *et al*, 2005). These patients experience recurrent flares of fever and inflammation in their joints and skin. The causes underlying these symptoms are still poorly defined (Majeed *et al*, 1989; Ferguson & El-Shanti, 2021).

1 Instituto de Biología y Genética Molecular, Consejo Superior de Investigaciones Científicas (CSIC), Valladolid, Spain

2 Centro de Investigación Biomédica en Red de Diabetes y Enfermedades Metabólicas Asociadas (CIBERDEM), Instituto de Salud Carlos III, Madrid, Spain

3 Immunology Unit, Department of Biomedical Sciences, Faculty of Medicine and Health Sciences, University of Barcelona, Barcelona, Spain

4 Institut d'Investigacions Biomèdiques August Pi i Sunyer, Barcelona, Spain

5 Departamento de Medicina Preventiva y Salud Pública, Facultad de Medicina, Universidad Autónoma de Madrid, Madrid, Spain

\*Corresponding author. Tel: +34 983 184 833; E-mail: [mbalboa@uva.es](mailto:mbalboa@uva.es)

†These authors contributed equally to this work

In general, autoinflammatory diseases develop subsequent to dysregulated activation of innate immune cells (McDermott *et al.*, 1999; Tartey & Kanneganti, 2020). We have recently described that macrophages defective in lipin-2 exhibit an exacerbated production of IL-1 $\beta$  due to increased classical activation of the NLRP3 inflammasome (Lordén *et al.*, 2017; Balboa *et al.*, 2019). Inflammasomes are intracellular machineries, key in the battle against pathogens, that assemble to activate caspase-1 (Martinon *et al.*, 2002). Once caspase-1 is activated, it cleaves pro-IL-1 $\beta$  and pro-IL-18 to produce the mature cytokines. In macrophages, two different signals are needed for IL-1 $\beta$  production through the NLRP3 inflammasome (Bauernfeind *et al.*, 2009; Franchi *et al.*, 2009). The first signal is generated by the binding of PAMPs to Toll-like receptors (TLRs) or cytokines like TNF- $\alpha$ . This upregulates *IL1B* through activation of transcription factors such as NF- $\kappa$ B. The second signal is generated by cellular events such K<sup>+</sup> efflux and mitochondria or lysosome damage.

Canonical activation of the NLRP3 inflammasome in macrophages occurs through sequential exposure of the cells to bacterial lipopolysaccharide (LPS, TLR4 ligand—first signal) and ATP (P2X<sub>7</sub> receptor ligand—second signal). The absence of lipin-2 leads to enhanced LPS signaling that augments pro-IL-1 $\beta$  production, and increased K<sup>+</sup> efflux due to over-activation of P2X<sub>7</sub> receptors (Lordén *et al.*, 2017). While these findings establish that lipin-2 acts as a brake to control the extent of inflammation, many questions are still open. One of these refers to the way innate immune cells, particularly macrophages, regulate the expression of lipin-2. This is a key question to solve because it may provide important clues as to where and when does lipin-2 exert its anti-inflammatory and metabolic regulatory roles and, perhaps, aid in the development of strategies aimed to better manage the symptoms of Majeed disease.

In this study, we show that *Lpin2* is upregulated by IFNs through STAT1, and this constitutes a key event for the latter to express their antiviral activity. We also demonstrate that lipin-2 protects mitochondria from oxidative damage and reduces mtDNA release, thereby providing a mechanism to explain its anti-inflammatory actions during NLRP3 activation by intracellular viral molecular patterns. Further, we show that symptomatic patients infected with SARS-CoV-2, the virus responsible for the COVID-19 pandemic, can be distinguished from asymptomatic patients on the basis of their very different lipin-2 expression levels. Collectively, our study

suggests that: (i) unexplained recurrent flares of symptoms in Majeed patients, and more specifically their high IL-1 $\beta$  levels, could be due to otherwise unnoticed viral infections; (ii) inhibitors of mtDNA release can be helpful in the management of Majeed disease; and (iii) measuring *LPIN2* levels may be useful to identify higher-risk COVID-19 patients.

## Results

### TLRs and IFNs regulate the expression of lipin-2 in BMDMs

We began this study by analyzing whether the engagement of classical PRRs such as the TLRs promotes changes in the expression levels of lipin-2 in innate immune cells. To this end, we stimulated bone marrow derived macrophages (BMDMs) with known TLR agonists and analyzed the expression of lipin-2 by immunoblot. The antibody against lipin-2 used in the present study recognizes a ~ 140 kDa band. This antibody has previously been used by others in murine macrophage cell lines (Watahiki *et al.*, 2020). Lipin-2 is heavily phosphorylated in cells. This radically changes its electrophoretic mobility from a predicted 95 kDa band to the observed ~ 140 kDa band in SDS-PAGE (Eaton *et al.*, 2014). The results showed that agonists of TLR1/2 (Pam3CSK4), TLR2 (lipoteichoic acid, LTA), TLR3 (poly(I:C)), TLR4 (LPS), TLR5 (Flagellin), TLR2/6 (FSL-1), TLR7 (imiquimod) and TLR9 (ODN1826) upregulated lipin-2 expression to various degrees (Fig 1A and Appendix Fig S1). The specificity of the antibody used to detect lipin-2 was verified by analyzing lysates from *Lpin2*<sup>-/-</sup> macrophages (Fig 1B). In these cells, the antibody failed to detect a 140 kDa band (Fig 1B). Conversely, in cells overexpressing lipin-2 the antibody recognized the expected 140 kDa band (Appendix Fig S2). As a positive control that cells were activated properly by all TLR stimuli used, we also investigated the expression of proteins known to be upregulated by TLRs, such as COX-2 and viperin. The levels of both proteins increased in cells stimulated with all the agonists (Fig 1A). Time-course analyses of lipin-2 expression in cells activated with different TLR agonists indicated that the enzyme experienced measurable increases in expression at different time points after stimulation, reaching a plateau of expression between 8 and 18 h depending on the TLR activated (Fig 1C and D, and Appendix Fig S1).

**Figure 1. Effect of TLR agonists and interferons on lipin-2 expression.**

- A BMDMs were treated or not (control) with 1  $\mu$ g/ml Pam3CSK4 (TLR1/2), 1  $\mu$ g/ml LTA (TLR2), 25  $\mu$ g/ml poly(I:C) (TLR3), 200 ng/ml LPS (TLR4), 100  $\mu$ g/ml FSL-1 (TLR6/2), 5  $\mu$ g/ml Imiquimod (TLR7) or 1  $\mu$ M ODN 2395 (TLR9) for 24 h. Cells lysates were analyzed by immunoblot using specific antibodies against lipin-2, COX-2, viperin, and  $\beta$ -tubulin as a loading control. Quantifications of the bands relative to  $\beta$ -tubulin and normalized to Control cell values are shown on the right.
- B Homogenates from Wt and *Lpin2*<sup>-/-</sup> BMDMs were analyzed by immunoblot using antibodies against lipin-2 and  $\beta$ -tubulin (loading control).
- C, D BMDMs were treated with 200 ng/ml LPS (C) or 25  $\mu$ g/ml poly(I:C) (D) for the indicated periods of time. Quantifications of the bands relative to  $\beta$ -actin and normalized to time zero values are shown on the right.
- E–H BMDMs were treated with 500 U/ml IFN- $\beta$  (E) or 200 U/ml IFN- $\gamma$  (G) for the indicated periods of time, or with the indicated concentrations of IFN- $\beta$  (F) or IFN- $\gamma$  (H) for 24 h. Homogenates were analyzed by immunoblot using antibodies against lipin-2 and  $\beta$ -actin (loading control). Quantifications of the bands relative to  $\beta$ -actin and normalized to time zero or untreated cells are shown on the right.
- I Wt or *Ifnar1*<sup>-/-</sup> BMDMs were treated or not (control) with 200 ng/ml LPS, 25 ng/ml poly(I:C), or 500 U/ml IFN- $\beta$  for 24 h. Homogenates were analyzed by immunoblot using antibodies against lipin-2 and  $\beta$ -actin (loading control). Quantifications of the bands relative to  $\beta$ -actin and normalized to Wt control cells are shown on the right. Shown are representative experiments of at least two independent ones. \**P* < 0.05; \*\**P* < 0.01; \*\*\**P* < 0.001, ####*P* < 0.001.

Data information: The immunoblots in (A, C, D, F, and I) are representative examples from three biological replicates. The immunoblots in (E, G, and H) are representative examples from five biological replicates. Two different experiments were performed. Data represent the mean  $\pm$  SEM. *P*-value of one-way ANOVA followed by Holm-Sidak test (A) or Student's *t*-test (C–I). \**P* < 0.05; \*\**P* < 0.01; \*\*\**P* < 0.001, ####*P* < 0.001. \*, treated vs. control cells (unstimulated or time = 0), # Wt vs. *Ifnar1*<sup>-/-</sup> cells. Source data are available online for this figure.

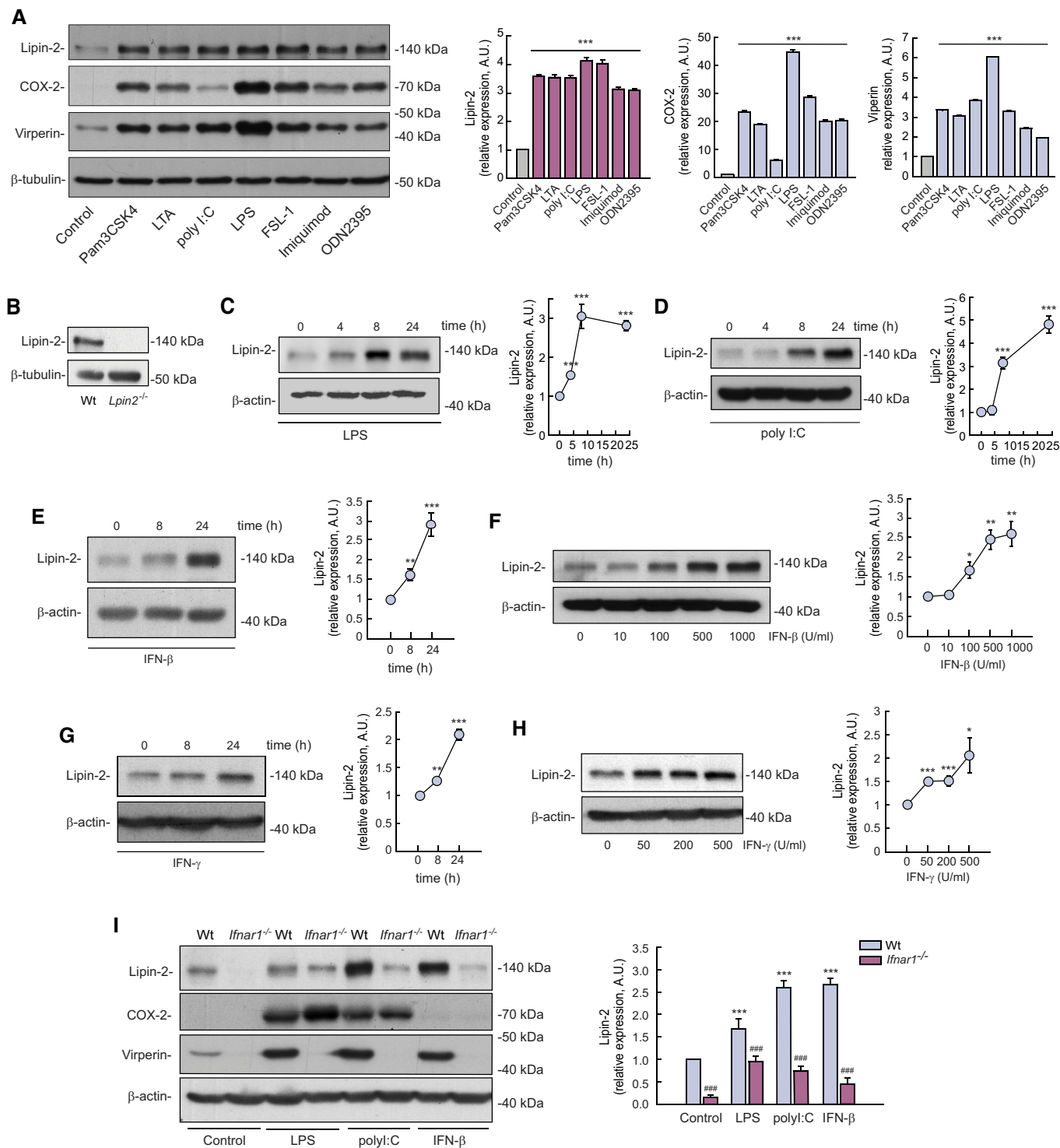


Figure 1.

The finding that a delay exists before lipin-2 levels start to increase after TLR activation suggests the existence of a factor that is produced prior to and intermediates in the process. Because a number of TLR receptors, including TLR3, TLR4, TLR7, and TLR9 are strong inducers of IFN expression (Chow *et al*, 2015), we sought to study the possible involvement of IFN in regulating lipin-2 expression in macrophages. As shown in Fig 1E–H, treating BMDMs

with IFN-β or IFN-γ increased the expression of lipin-2 in a time and dose-dependent manner. Importantly, cells deficient in the IFN-β receptor subunit 1 (*Ifnar1*) displayed reduced expression levels of lipin-2, and their capacity to increase lipin-2 levels after TLR activation or IFN-β treatment was significantly reduced (Fig 1I). These results indicate that both basal and stimulated IFN levels impact on lipin-2 expression.

To ascertain whether lipin-2 levels were regulated at the protein or mRNA level, we studied the levels of *Lpin2* mRNA during cellular stimulation by analyzing gene expression arrays (Raza et al, 2014a; Data ref: Raza et al, 2014b). We found that LPS and IFNs increased *Lpin2* mRNA levels in a time-dependent manner, while the mRNA levels for other members of the lipin family of enzymes, i.e. *Lpin1* and *Lpin3*, were decreased or unchanged respectively (Appendix Fig S3). We confirmed these results in IFN- $\beta$ - and IFN- $\gamma$ -treated BMDMs, by evaluating by qPCR the expression levels of *Lpins* and also those of *Rsad2/viperin* and *Irf7*, two well-known ISGs (Fig 2A and B). The data showed that among lipins, *Lpin2* selectively increased its mRNA levels during macrophage stimulation with TLR agonists and by IFNs.

### STAT1 participates in the transcriptional upregulation of *Lpin2*

In the next series of experiments, the events controlling *Lpin2* upregulation by IFNs were investigated. We used actinomycin D and cycloheximide to inhibit transcription and translation, respectively. The results indicated that transcription is necessary to increase *Lpin2* mRNA levels and that both transcription and translation events are needed for lipin-2 expression to increase during macrophage activation by IFN- $\beta$  (Fig 2C and D). To further demonstrate the involvement of IFN in the transcriptional activation of *Lpin2*, we analyzed newly transcribed levels of *Lpin2* mRNA by gene expression arrays (Dölken et al, 2008; Data ref: Robertson & Ghazal, 2016). The results showed that IFN- $\gamma$  induces the transcription of new mRNA for *Lpin2* (Appendix Fig S4).

Next, the signaling events that participate in *Lpin2* mRNA upregulation were evaluated. Engagement of IFN receptors initiates signaling events through activation of JAK1 and TYK2 (IFNAR) or JAK1 and JAK2 (IFNGR). Subsequently, IFNGR activates STAT1, while IFNAR activates STAT1 and STAT2, and both receptors can secondarily activate STAT3 (Stark & Darnell Jr, 2012). We analyzed first the effect of the selective JAK1/2 inhibitor ruxolitinib on lipin-2 expression. Treatment of BMDMs with ruxolitinib completely abolished the induction of *Lpin2* mRNA, as well as the increases in lipin-2 protein levels by IFN- $\beta$  (Fig 2E and F). In contrast, nifuroxazide, a STAT3 inhibitor (Nelson et al, 2008), had no effect. The same behavior was found in BMDMs activated with the TLR3 agonist poly(I:C), thus suggesting the key involvement of JAKs in mediating IFN-induced lipin-2 expression (Appendix Fig S5).

It has previously been shown that lipin-2 levels can be regulated by ubiquitination and proteasome degradation (Watahiki et al, 2020). We studied the effect of the proteasome inhibitor MG132 on the capacity of IFN- $\beta$  to increase lipin-2 expression levels. We found that the inhibitor did not increase the levels of expression of lipin-2, indicating that a decreased proteolysis by the proteasome does not play a role in the increased expression of the enzyme in this scenario.

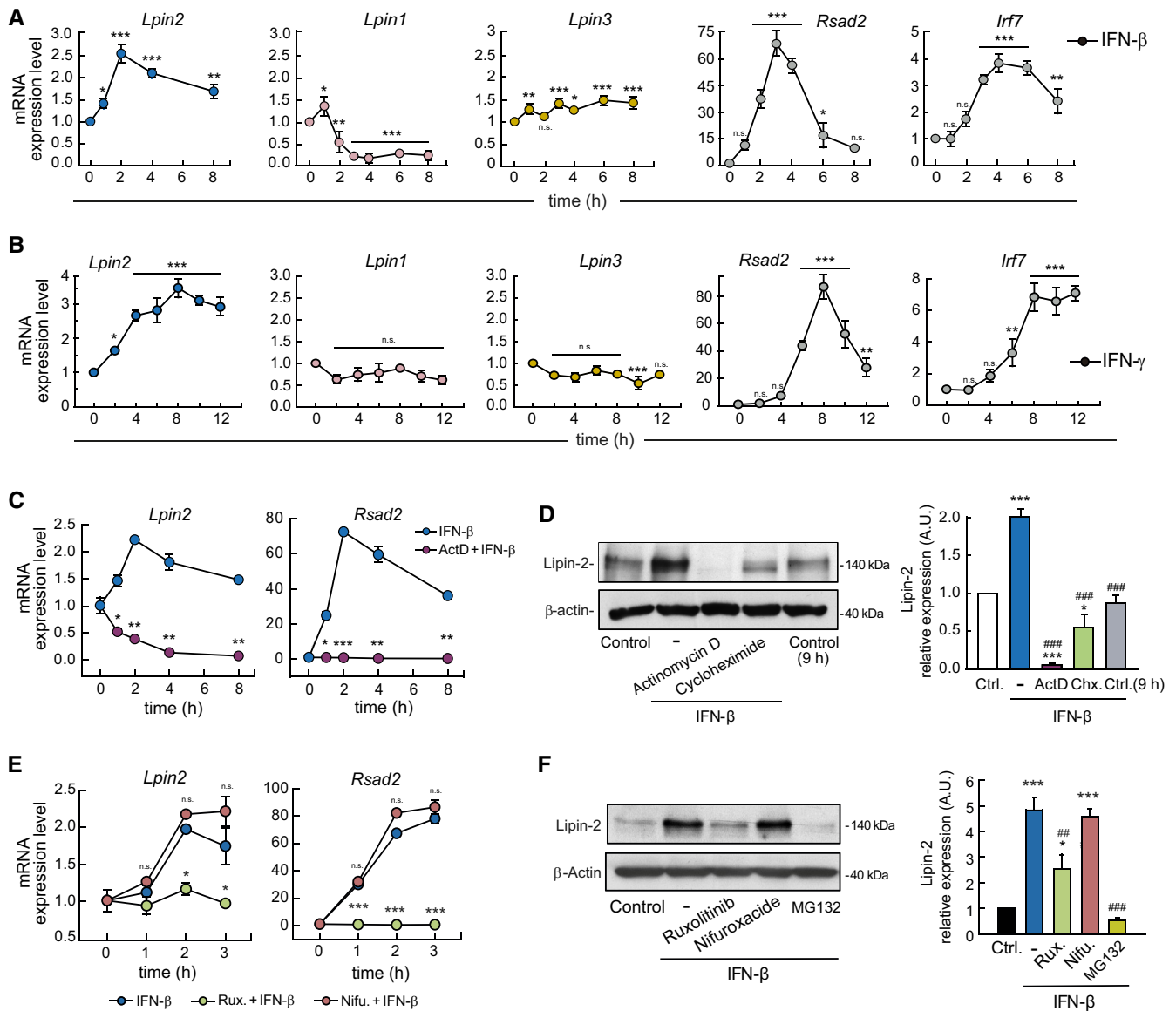
To assess the role of STAT1 in *Lpin2* transcriptional regulation, we analyzed gene expression array data from STAT1<sup>-/-</sup> BMDMs stimulated with IFN- $\gamma$  (Semper et al, 2014a; Data ref: Semper et al, 2014b). The data showed that, in the absence of STAT1, the ability of IFN- $\gamma$  to increase *Lpin2* mRNA levels is abolished (Fig 3A). To study whether the transcriptional activation of *Lpin2* correlates with binding of STAT1 to the *Lpin2* locus, we performed analyses of ChIP-seq data from BMDMs stimulated with IFN- $\beta$  and IFN- $\gamma$  (Ng

et al, 2011a; Data ref: Ng et al, 2011b). The results presented in Fig 3 indicate that STAT1 binds to three different sequences in the locus of *Lpin2* (peaks 1, 2 and 3). The first peak is around 5 kb upstream of the initiation of the transcription, while the second and third peaks are located downstream, between the first and second exons, at around 7.8 and 8.2 kb respectively of the initiation of the transcription (Fig 3B). Analysis of the density of reads in each peak showed that STAT1 is already attached to peak 1 in unstimulated cells, and treatment with IFN- $\gamma$  but not IFN- $\beta$ , increases the number of reads to this region, indicating an enhanced binding of STAT1 to this sequence (Fig 3B and C). In contrast, STAT1 is almost absent of peak 2 in unstimulated cells, but both IFNs promote its binding to this region, with IFN- $\beta$  being more potent in this regard. Finally, only IFN- $\beta$  appears to significantly induce STAT1 binding to the sequence present in peak 3. Under these experimental conditions, *Lpin2* mRNA levels were induced by both IFN- $\beta$  and IFN- $\gamma$  (Fig 3D).

Analysis of the sequences of the STAT1 peaks found in the *Lpin2* locus revealed the presence of GAS consensus motifs in the three peaks, and a unique ISRE consensus motif in peak 2 (Appendix Fig S6). These data suggest that IFN- $\gamma$  promotes the binding of STAT1 to GAS sequences in peaks 1 and 2, while IFN- $\beta$  induces the binding of STAT-1 to the ISRE/GAS sequences found in peak 2, and to the GAS sequence found in peak 3. In addition to inducing the formation of ISGF3, it has been reported that IFN- $\beta$  may promote the dimerization of STAT1 (GAF) (Ivashkiv & Donlin, 2014). This event may help explain the induction of STAT1 binding to GAS sequences present in the *Lpin2* locus during IFN- $\beta$  stimulation of BMDMs (Fig 3B and C). Altogether, the data illustrate the participation of STAT-1 in the induction of *Lpin2* transcription by IFN.

### Lipin-2 controls viral replication

One of the key functions of IFNs is to control viral infections through the transcriptional induction of ISGs. Given the regulation of lipin-2 expression by IFNs, we went on to assess whether the phosphatase plays a role in the antiviral response. For these experiments, we chose murine CMV (MCMV) because IFN signaling is crucial for the control of its infection *in vivo* (Lio et al, 2016). Accordingly, we first evaluated whether MCMV-infected BMDMs were able to increase *Lpin2* mRNA levels (Blanc et al, 2013; Data ref: Blanc et al, 2015). Figure 4 shows that this was the case. The effect was particularly noteworthy after 3 h of infection, and occurred in parallel with well-known ISGs like *Rsad2* or *Irf7*. In contrast, *Lpin1* and *Lpin3* were not substantially increased under these conditions (Fig 4A). We confirmed by qPCR that macrophage infection by MCMV increased *Lpin2* expression (Fig 4B). To assess whether lipin-2 had any influence on virus replication, we infected BMDMs with an MCMV carrying the GFP gene (MCMV-GFP), and GFP fluorescence was analyzed in the cultures at different times post-infection. Infected wild type BMDMs experienced a progressive increase in fluorescence after a 3-day infection period (Fig 4C). Importantly, lipin-2-deficient macrophages manifested higher increases in fluorescence than wild type cells from days 2–6 after infection. This indicated enhanced viral replication. To verify whether the increase in replication was accompanied by an augmented production of infective viral particles in *Lpin2*<sup>-/-</sup> macrophages, supernatants of infected macrophages were collected and viral infectivity was analyzed on mouse embryonic fibroblast



**Figure 2. *Lpin2* mRNA levels are controlled by interferons.**

A, B BMDMs were treated with 500 U/ml IFN-β (A) or 200 U/ml IFN-γ (B) for the indicated periods of time. mRNA levels for the indicated genes were analyzed by qPCR, using *Gapdh* as reference and normalized to time zero.

C BMDMs were treated with 500 U/ml IFN-β in the presence or absence of 1 μg/ml Actinomycin D (ActD). mRNA levels were analyzed by qPCR, using *Gapdh* as reference and normalized to time zero.

D BMDMs were left untreated (Control and Control 9 h) or treated with 500 U/ml IFN-β in the absence or presence of 1 μg/ml Actinomycin D (ActD) or 10 μg/ml Cycloheximide (Chx). Cellular homogenates were analyzed by immunoblot using antibodies against lipin-2 and β-actin (loading control). Quantifications of the bands relative to β-actin and normalized to Control cells are shown on the right.

E, F BMDMs were untreated (Control) or treated with 500 U/ml IFN-β in the presence or absence of 5 μM Ruxolitinib (Rux.), 10 μM Nifuroxazide (Nifu.) or 20 μM MG132 (only in F). mRNA levels were analyzed by qPCR, using *Gapdh* as reference and normalized to time zero. (E) Cellular homogenates were analyzed by immunoblot using antibodies against lipin-2 and β-actin (loading control) (F). Quantifications of the bands relative to β-actin are shown on the right.

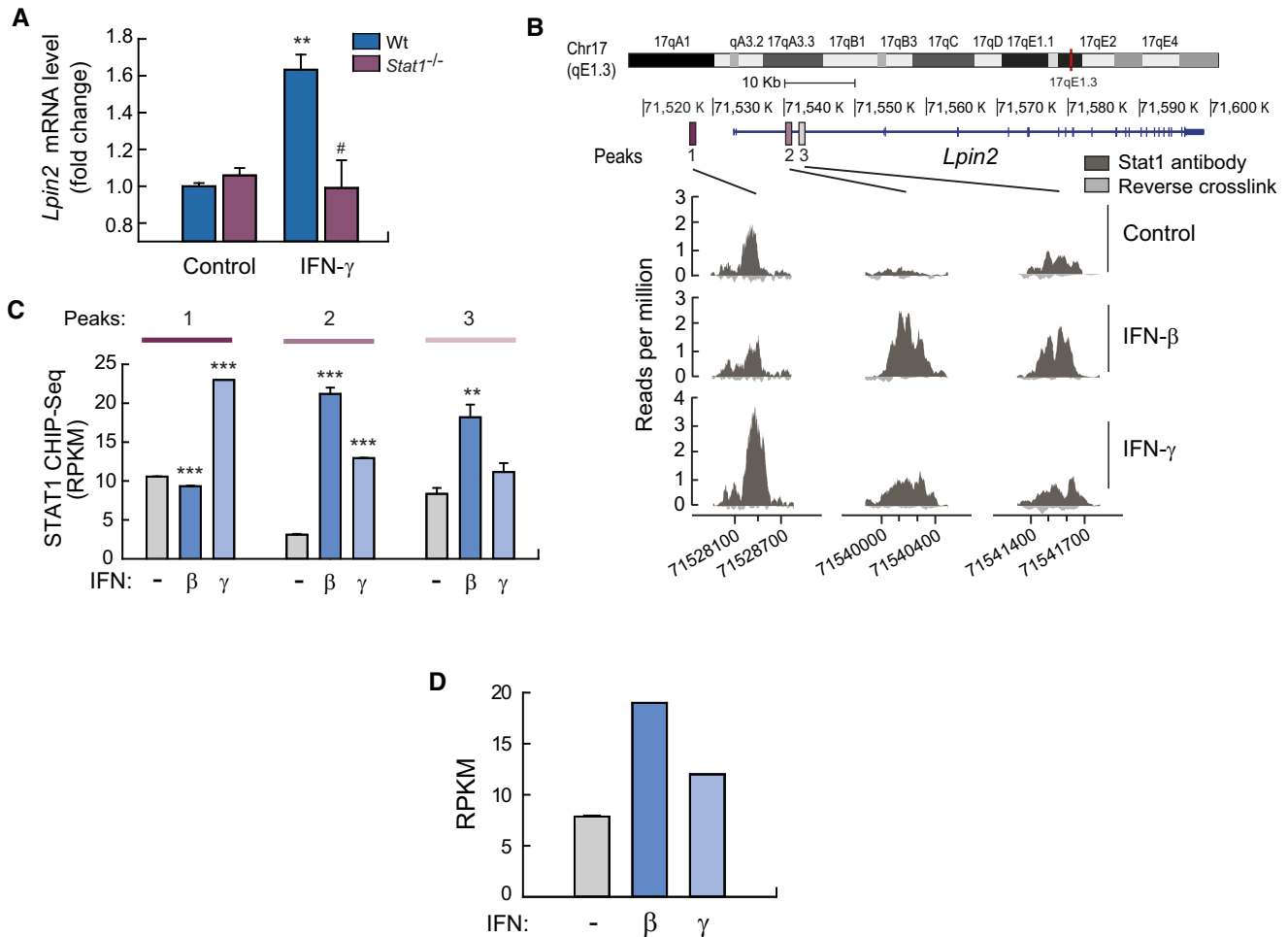
Data information: Data from (A–C and E) are shown as means ± SEM of biological triplicates. Two experiments were performed. The immunoblots in (D, F) are representative examples from three biological replicates. Data represent the mean ± SEM. *P* value of one-way ANOVA followed by Holm-Sidak test (A, B, D, F), or Student's *t*-test (C, D). (A, B) \*, IFN-treated vs. time = 0. (C) \*, IFN-β vs. ActD+IFN-β. (E) \*, IFN-β vs. Rux + IFN-β or Nifu+IFN-β. (D, F) \*, IFN-β treated vs. control cells; # conditions indicated vs. just IFN-β treated. n.s., not significant; \**P* < 0.05; \*\**P* < 0.01; \*\*\**P* < 0.001; ####*P* < 0.01; #####*P* < 0.001.

Source data are available online for this figure.

(MEFs) monolayers. Macrophage lipin-2 deficiency caused a significant increase in fluorescence forming units (FFUs) (Fig 4D). The same results were also observed when the infectivity of the

supernatants collected at different times from the infected macrophages was analyzed by standard plaque assays on MEFs (Fig 4E).





**Figure 3. STAT-1 binds to *Lpin2* locus to participate in its transcriptional upregulation during interferon stimulation.**

**A** Wt and STAT1<sup>-/-</sup> BMDMs were left untreated (Control) or treated with 100 U/ml IFN- $\gamma$  for 6 h, and gene expression was analyzed by microarrays. Fold change respect to Wt control cells are shown. Data are from triplicate samples and represent means  $\pm$  SEM. \*\* $P < 0.01$ , # $P < 0.05$  by Student's *t*-test. \*, IFN- $\gamma$  treated vs. control cells; # STAT1<sup>-/-</sup> vs. Wt cells.

**B** BMDMs were left untreated (Control) or treated with IFN- $\beta$  or IFN- $\gamma$  for 6 h and Chip-seq analysis was performed using anti-STAT1 antibodies. Shown are the main three STAT1 peaks called by MACS associated to the *Lpin2* locus (dark gray). Reads from just reverse crosslink is also shown (light gray).

**C** Shown are Chip-seq reads per kilobase per million reads (RPKM) values for STAT1-binding peaks associated with *Lpin2* relative to input controls. Statistics were performed with respect to unstimulated samples (-) for each peak. \*\* $P < 0.01$ ; \*\*\* $P < 0.001$  by Student's *t*-test.

**D** BMDMs were left untreated (-) or treated with IFN- $\beta$  or IFN- $\gamma$  for 6 h, and gene expression was analyzed by RNA-seq. Data are shown as RPKM for peaks associated to *Lpin2*.

Source data are available online for this figure.

To further establish the involvement of lipin-2 in MCMV replication, experiments were conducted in lipin-2-silenced RAW 264.7 macrophages (treated with specific siRNAs). These experiments confirmed that MCMV replicate better when lipin-2 levels are decreased (Fig 4F). These data support the notion that acute elimination of lipin-2 is sufficient to produce the observed effects on viral behavior.

To study whether these results could be translated to animal models of infection, mice were infected with MCMV for 5 days, and viral titers were determined in liver and spleen, two primary organs for viral replication. In agreement with the *in vitro* data, we observed that lipin2-deficient animals display a higher viral load in both organs (Fig 4G). Collectively, these data suggest that the

induction of *Lpin2* expression during MCMV infection plays a role in the control of viral replication.

We also tested whether lipin-2 participates in the control of viruses that are known to restrain IFN production and the anti-viral activity promoted by several ISGs, such as Vaccinia virus (VACV) (Smith *et al*, 2018). As expected, replication of VACV in infected BMDMs was not affected by the phosphatase (Appendix Fig S7).

#### Lipin-2 controls inflammation during virus-derived nucleic acid recognition

Beyond their role in anti-viral defense, IFNs have also been described as modulators of immunopathogenic events curtailing

collateral damage during infection (Lee & Ashkar, 2018). Thus we evaluated whether lipin-2, as a part of the IFN response, was involved in decreasing the inflammation during viral recognition by macrophages. IL-1 $\beta$  is a key cytokine during inflammatory reactions. IL-1 $\beta$  is essential for the host response to pathogens, but is also fully capable of generating damage when produced at too high levels (Masters et al, 2009). We evaluated whether the presence of lipin-2 affected IL-1 $\beta$  production by BMDMs treated sequentially with poly(I:C) (viral nucleic acid mimetic) and ATP (to activate the inflammasome). Lipin-2-deficient BMDMs produced much higher levels of IL-1 $\beta$  than wild type cells (Fig 5A). This correlated with increased levels of *I1b* mRNA during poly(I:C) stimulation in *Lpin2*<sup>-/-</sup> BMDMs and silenced RAW264.7 macrophages (Fig 5B and

Appendix Fig S8). Importantly, the same behavior was also found in *LPIN2*-silenced primary human macrophages (Fig 5C). The participation of TLR3 in the upregulation of *I1b* mRNA expression was confirmed by silencing the receptor in BMDMs (Fig 5D). Analysis of the signal transduction events implicated showed that NF- $\kappa$ B (p65) experienced a quicker translocation to the nucleus in lipin-2-deficient cells compared with lipin-2 expressing cells. This indicated an earlier activation of this factor during poly(I:C) stimulation (Fig 5E). TLR3 signaling is also known to involve MAPK activation (Janeway Jr & Medzhitov, 2002). Evaluation of ERK, JNK and p38 phosphorylation by immunoblot showed that the activation of all of these kinases was also ahead of time in lipin-2-deficient macrophages (Fig 5F). We also found that MAPK inhibitors (PD98059 for

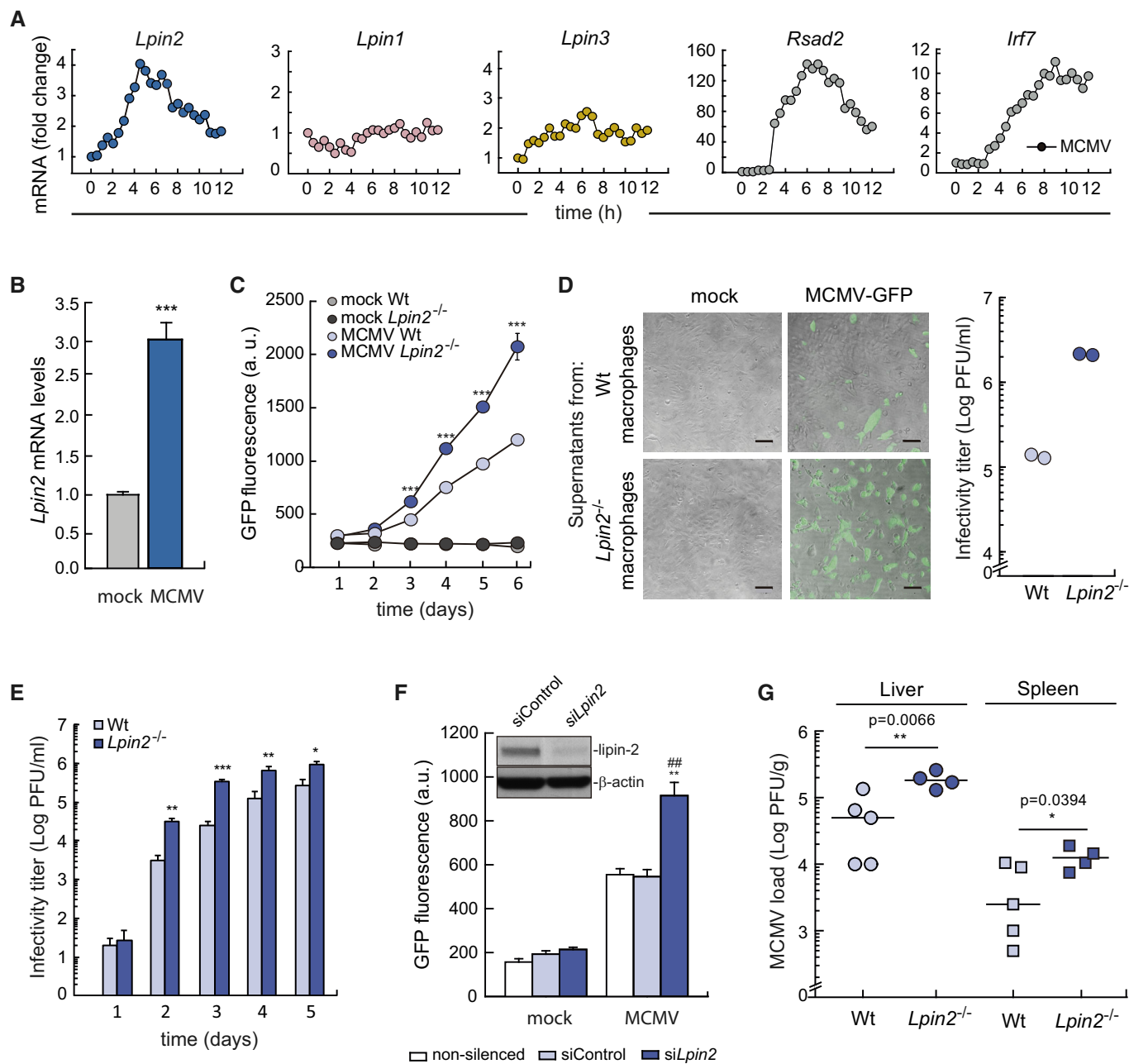


Figure 4.

**Figure 4. Lipin-2 restricts MCMV replication *in vitro* and *in vivo*.**

- A BMDMs were infected with MCMV (MOI = 1) for the indicated time points. Gene expression was analyzed by microarrays. Data are from a single biological replicate at each time point. Data shows fold gene expression change respect to expression levels at 0 h.
- B BMDMs were infected with MCMV (MOI = 1) for 4 h and mRNA levels for *Lpin2* were quantified by qPCR, using *Gapdh* as reference. Data were normalized to mock infected cells. Data from biological triplicate samples are represented as mean  $\pm$  SEM. \*\*\* $P$  < 0.001, Student's *t*-test.
- C BMDMs from Wt or *Lpin2*<sup>-/-</sup> animals were mock infected or infected with MCMV-GFP (MOI = 2) for 2 h. GFP fluorescence present in cell cultures was analyzed at the indicated time points after infection. Data from biological triplicate samples are represented as means  $\pm$  SD. \*\*\* $P$  < 0.001, Student's *t*-test.
- D BMDMs from Wt or *Lpin2*<sup>-/-</sup> animals were mock infected or infected with MCMV-GFP (MOI = 4). Supernatants were collected at day 3 post infection and, either transferred to MEF monolayers which were examined by microscopy 24 h post-infection (left panels) or titrated by standard plaque assays on MEFs, determining the number of FFU under the microscope (right panel). Scale bars: 100  $\mu$ m.
- E BMDMs from Wt or *Lpin2*<sup>-/-</sup> animals were mock infected or infected with MCMV-GFP (MOI = 2), supernatants were collected at different times after infection and titrated by standard plaque assays on MEFs, counting PFU under the microscope. Data from biological triplicate samples are represented as mean  $\pm$  SD. \* $P$  < 0.5, \*\* $P$  < 0.01, \*\*\* $P$  < 0.001, Student's *t*-test.
- F RAW264.7 cells silenced for *Lpin2* or not were mock infected or infected with MCMV-GFP (MOI = 2). GFP fluorescence present in cell cultures was analyzed 5 days after infection. Data from biological triplicate samples are represented as mean  $\pm$  SEM. \*\* $P$  < 0.01, ### $P$  < 0.01, Student's *t*-test. \* *siLpin2* vs. siControl, # *siLpin2* vs. unsilenced cells. The insert shows lipin-2 expression in silenced cells by immunoblot.
- G Wt ( $n$  = 5) and *Lpin2*<sup>-/-</sup> ( $n$  = 4) animals were intraperitoneally injected with MCMV ( $3.5 \times 10^6$  PFU per mouse) and, after 4 days of infection viral titers were analyzed in the liver and the spleen of animals by standard plaque assays, counting PFUs. Statistical differences were tested by Student's *t*-test, and *P*-values are shown.

Source data are available online for this figure.

MEK, the kinase upstream of ERK; SP600125 for JNK, and SB203580 for p38), significantly reduced the expression levels of *Il1b* mRNA in macrophages expressing or not lipin-2. The most efficient of these was the p38 inhibitor (SB203580) (Fig 5G). We next evaluated whether the expression levels of proteins that participate in inflammasome activation, the cytosolic machinery that ultimately activates caspase-1 to proteolytically mature pro-IL-1 $\beta$ , could also be enhanced in lipin-2-deficient macrophages during the poly(I:C) challenge. Both NLRP3 expression (inflammasome receptor) and mRNA levels for *Casp1* (caspase-1) were increased under these circumstances (Fig 5H and I). As a consequence of the increased signaling through TLR3 that characterized cells deficient in lipin-2, we also found that, after poly(I:C) stimulation, they displayed increased expression levels for TLR3 itself. Other ISGs such as *Ifih1*/MDA5, *Ddx58* (RIG-I), and *Eif2ak2* (PKR), which are intracellular receptors for dsRNA, and *Rsad2*/viperin, a dual role factor for viral host defense (West *et al*, 2015), were also found to be elevated.

Collectively, these results show that lipin-2 regulates the production of IL-1 $\beta$  as well as ISGs expression levels by regulating the signal transduction events that occur downstream of TLR3 engagement.

**Lipin-2 controls NLRP3 inflammasome activation induced by transfected poly(I:C)**

To investigate whether viral nucleic acid mimetics can provide the second signal for inflammasome activation, we transfected primed macrophages with poly(I:C), to make it accessible to intracellular receptors such as the inflammasomes, and studied IL-1 $\beta$  production. The results showed that, when transfected with poly(I:C), primary human macrophages, BMDMs, and RAW264.7 macrophage-like cells all increased IL-1 $\beta$  levels. Importantly, the absence of lipin-2 further enhanced the response (Fig 6A–C). IL-1 $\beta$  production was dependent on the dose of transfected poly(I:C) (Fig 6D).

**Figure 5. Lipin-2 controls inflammasome priming by molecules that mimic viral nucleic acids.**

- A BMDMs from Wt or *Lpin2*<sup>-/-</sup> animals were left untreated, primed with 10  $\mu$ g/ml of poly(I:C) for 4 h and activated or not with 2 mM ATP for 4 or 8 h, as indicated. IL-1 $\beta$  levels present in cell supernatants were quantified by specific ELISAs.
- B BMDMs from Wt or *Lpin2*<sup>-/-</sup> animals were left untreated or treated with 10  $\mu$ g/ml poly(I:C) for 4 and 8 h. mRNA levels for *Il1b* were analyzed by qPCR, using *Gapdh* as reference and normalized to time zero.
- C Primary human macrophages, nucleofected with control siRNAs (siControl) or against *LPIN2* (*siLPIN2*), were treated or not with 25  $\mu$ g/ml poly(I:C) for 4 h and mRNA levels for *IL1B* (left panel) or *LPIN2* (right panel) were analyzed by qPCR. *ACTB* was used as reference.
- D BMDMs from Wt or *Lpin2*<sup>-/-</sup> animals were transfected with control siRNAs or against TLR3 (*siTLR3*) and left untreated or stimulated with 10  $\mu$ g/ml of poly(I:C) for 4 h. mRNA levels for *Il1b* (left panel) or *TLR3* (right panel) were analyzed by qPCR, using *Gapdh* as reference.
- E RAW264.7 cells silenced for *Lpin2* or not were treated with 25  $\mu$ g/ml of poly(I:C) for the indicated times. Cells were immunostained using specific antibodies against p65. Nuclei were stained with DAPI. Images obtained by confocal microscopy are shown (left panel). Percentage of cells with nuclear p65 translocation is represented (right panel) ( $n$  = 60). Scale bars: 10  $\mu$ m.
- F Homogenates from RAW264.7 cells treated as in F were analyzed by immunoblot using antibodies against phospho-ERK, phospho-JNK and phospho-p38. Total ERK, JNK and p38 were used as a loading controls respectively. Densitometric quantification of the bands are represented in the lower panels.
- G RAW264.7 cells silenced for *Lpin2* or not were treated with 10  $\mu$ M of the indicated MAPK inhibitors prior to stimulation with 25  $\mu$ g/ml of poly(I:C) for 4 h. mRNA levels for *Il1b* were analyzed by qPCR, using *Gapdh* as reference.
- H RAW264.7 cells silenced for *Lpin2* or not were treated with 25  $\mu$ g/ml of poly(I:C) for the indicated periods of time. Cell homogenates were analyzed by immunoblot using specific antibodies against NLRP3 and  $\beta$ -actin. Densitometric quantification of the bands are represented in the lower panel.
- I RAW264.7 cells silenced for *Lpin2* or not were left untreated (Control) or stimulated with 25  $\mu$ g/ml of poly(I:C) for 4 h. mRNA levels for the indicated genes were analyzed by qPCR mRNA levels for *Il1b* were analyzed by qPCR, using *Gapdh* as reference.

Data information: Data shown in (A–D, F–I) from biological triplicate samples are represented as mean  $\pm$  SEM. (E) Data ( $n$  = 60) are represented as mean  $\pm$  SEM. Figures show representative experiments of two independent ones. \* $P$  < 0.05; \*\* $P$  < 0.01; \*\*\* $P$  < 0.001; # $P$  < 0.05; ### $P$  < 0.001, Student's *t*-test. \*, *Lpin2*-deficient vs. control cells; #, in (D), poly(I:C)-treated TLR3-deficient vs. poly(I:C)-treated siControl cells; #, in (G), cells treated with MAPKs inhibitors vs. just poly(I:C) treated cells. Source data are available online for this figure.



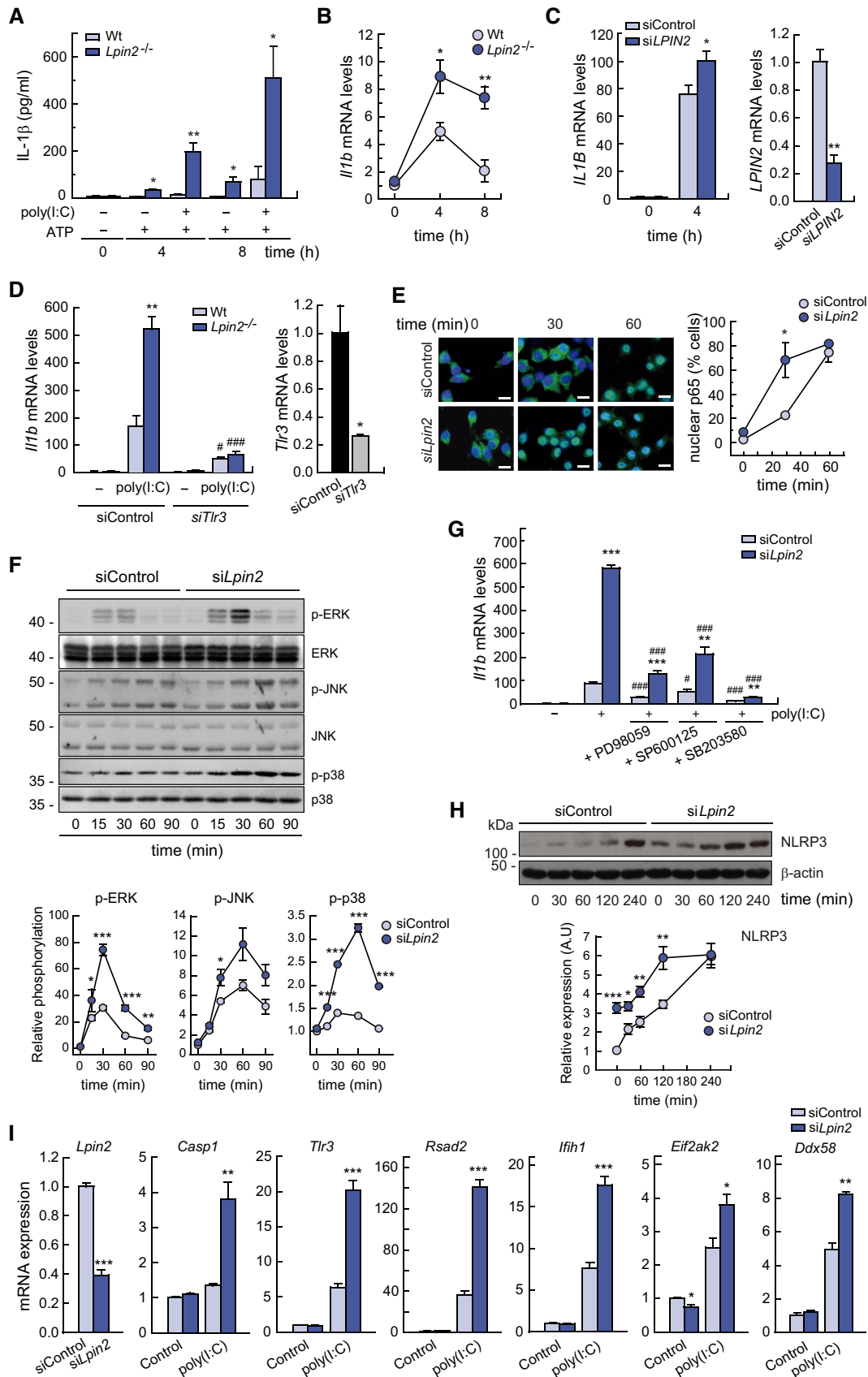


Figure 5.

*Il18* mRNA and pro-IL-18 levels are usually constitutive in cells (Gu et al, 1997). Conversion of pro-IL-18 to its mature form has been used as a reliable marker of inflammasome activation (Lordén et al, 2017). Analysis of IL-18 levels in poly(I:C)-transfected

macrophages showed an increase in cells deficient in lipin-2 (Fig 6E). We did not observe significant changes in *Il18* mRNA levels under these circumstances (Fig 6F). Immunoblot analyses of the supernatants of these cells confirmed the increase of IL-1 $\beta$

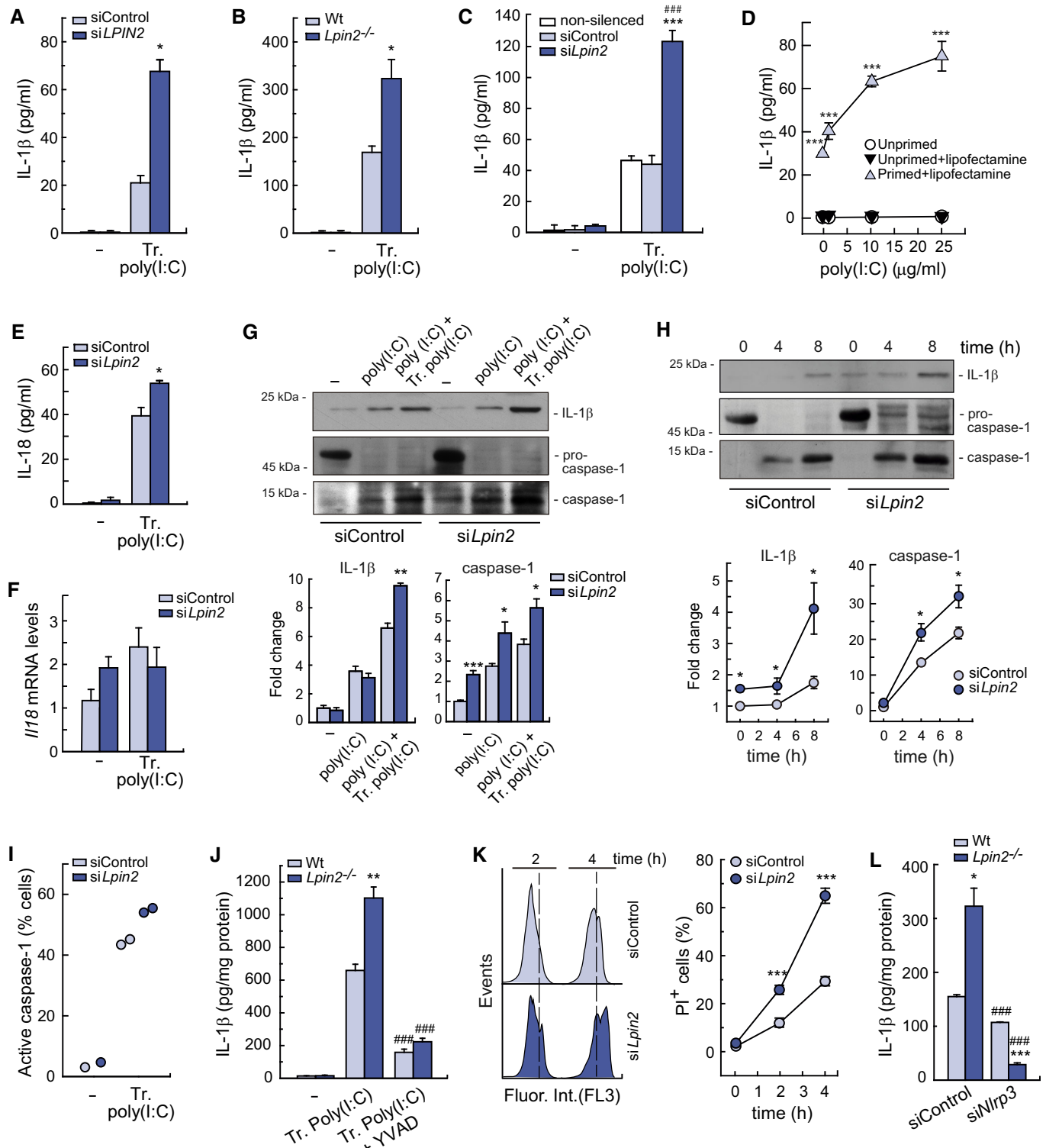


Figure 6.

**Figure 6. NLRP3 inflammasome activation by cytosolic poly(I:C) is regulated by lipin-2.**

- A–C Silenced primary human macrophages (A), Wt and *Lpin2*<sup>−/−</sup> BMDMs (B) or non-silenced/silenced RAW264.7 cells (C) were primed with 10 μg/ml poly(I:C) for 4 h and then transfected (Tr. poly(I:C) or not (−) with 10 μg/ml of poly(I:C) for 4 h. IL-1β present in cellular supernatants were quantified by specific ELISAs.
- D RAW264.7 cells were primed or not and then treated with different doses of poly(I:C) in the presence or absence of lipofectamine for 4 h. IL-1β present in cellular supernatants was quantified using a specific ELISA.
- E, F RAW264.7 cells silenced for *Lpin2* or not were transfected with 10 μg/ml of poly(I:C). IL-18 present in cellular supernatants was quantified using a specific ELISA (E), and *Il18* mRNA levels were quantified by qPCR, using *Gapdh* as reference (F).
- G, H BMDMs from Wt or *Lpin2*<sup>−/−</sup> animals were left untreated (−), primed with 10 μg/ml of poly(I:C) for 4 h (poly(I:C) and then transfected with 10 μg/ml of poly(I:C) (poly(I:C) + Tr. poly(I:C)) for 4 h (G), or the indicated periods of time (H). IL-1β and mature caspase-1 present in cellular supernatants from the same number of cells were analyzed by immunoblot. Densitometric quantification of bands is represented in lower panels.
- I RAW264.7 cells were treated as in (C). Cells were stained with FAM-FLICA during the last 60 min of activation and fluorescence was analyzed by flow cytometry. Data are shown as the percentage of cells with active caspase-1 (FAM-FLICA positive cells).
- J BMDMs were pretreated or not with 10 μM YVAD for 30 min and then treated as in (B). IL-1β present in cellular supernatants was quantified with a specific ELISA.
- K Primed RAW264.7 cells were transfected with 10 μg/ml of poly(I:C) for the indicated periods of time and assayed for PI permeability by flow cytometry. Right panel shows percentage of PI<sup>+</sup> cells.
- L BMDMs were silenced or not for *NLRP3*, primed and transfected with 10 μg/ml of poly(I:C) for 4 h. IL-1β present in cellular supernatants were quantified by specific ELISAs.

Data information: Data shown in (A–H, J–L) are from biological triplicate samples and are shown as mean ± SEM. Two independent experiments were performed. Data in I are from duplicate samples. \**P* < 0.05; \*\**P* < 0.01; \*\*\**P* < 0.001, \*\*\*\**P* < 0.0001, Student's *t*-test. For figures (A–C, E, and G–L): \*, lipin-2-deficient vs. control cells. For figure (D): \*, Cells primed+lipofectamine vs. unprimed. For (C): #, lipin2-deficient vs. unsilenced cells. For (J): #, Transfected poly(I:C) + YVAD vs. Transfected poly(I:C). For (L): #, siNLRP3 vs. siControl treated cells.

Source data are available online for this figure.

protein levels, especially in lipin-2-deficient cells (Fig 6G and H). Importantly, fragments of active caspase-1 were also present at elevated amounts in the supernatants of lipin-2-deficient cells, and appeared earlier than IL-1β (Fig 6G and H). Use of a fluorescent probe that specifically binds to active caspase-1 indicated that transfection of poly(I:C) promoted the activation of the protease, with higher levels being found in cells deficient in lipin-2 (Fig 6I). Further, inhibition of caspase-1 activity by the specific inhibitor Y-VAD blunted the production of IL-1β by transfected poly(I:C), and this occurred both in wild type and *Lpin2*<sup>−/−</sup> BMDMs (Fig 6J).

Caspase-1 is involved in a type of cell death called pyroptosis. Thus, macrophage cell death was evaluated in cells that had been first primed and then transfected with poly(I:C). For these experiments we took advantage of the property of propidium iodide to permeate damaged cell membranes. Flow cytometry data showed that lipin-2-deficient cells experienced higher levels of death than cells normally expressing the enzyme (Fig 6K). Finally, elimination of the inflammasome receptor NLRP3 by mRNA silencing reduced the capacity of BMDMs to release IL-1β, especially in cells from *Lpin2*<sup>−/−</sup>

mice (Fig 6L). Together, these data demonstrate that lipin-2 restrains NLRP3 inflammasome activation during recognition of cytosolic viral nucleic acid mimics.

**Lipin-2 regulates mtDNA release during cytosolic poly(I:C) recognition**

The presence of cytosolic mtDNA has been suggested as a key event for the activation of the NLRP3 inflammasome (Zhou *et al*, 2011; Zhong *et al*, 2018). To unveil possible mechanisms for the increased activation of the NLRP3 inflammasome by transfected poly(I:C), especially under reduced lipin-2 levels, we focused on studying whether cytosolic mtDNA is involved in the production of IL-1β in this model. Primed BMDMs, transfected with poly(I:C), were used to study cytosolic mtDNA levels in cytosolic fractions by analyzing the presence of the mtDNA-encoded gene *Dloop* (Fig 7A). Transfection of poly(I:C) increased the presence of *Dloop* in the cytosol of BMDMs, and this was augmented in cells from *Lpin2*<sup>−/−</sup> animals. To verify whether mtDNA was related to IL-1β production, we

**Figure 7. Lipin-2 controls inflammasome activation by reducing mtDNA release and ROS production.**

- A Primed BMDMs from Wt and *Lpin2*<sup>−/−</sup> animals were transfected or not (Control) with 10 μg/ml poly(I:C) for 4 h. Cytosol mtDNA levels were analyzed by qPCR as mentioned in M&M.
- B–D BMDMs from Wt and *Lpin2*<sup>−/−</sup> animals depleted or not of mtDNA (p<sup>0</sup>) were primed and transfected with 10 μg/ml poly(I:C) for 4 h. IL-1β present in cellular supernatants were quantified by specific ELISAs (B). Active caspase-1 and cell death were analyzed by flow cytometry after cell treatment with FAM-FLICA (C) or PI (D).
- E, F Primed BMDMs were transfected with 10 μg/ml poly(I:C) for 4 h and labeled with 10 μM DCFA (E) or 5 μM MitoSOX (F), and fluorescence was analyzed by flow cytometry. Right panels show the mean fluorescence intensities (MIF) observed in left panels.
- G RAW264.7 cells were silenced for *Lpin2*, treated with 10 μg/ml of poly(I:C) for 4 h, labeled with 10 μM DCFA, and analyzed by flow cytometry. Right panel shows the MIF observed in left panels.
- H Primed BMDMs from Wt and *Lpin2*<sup>−/−</sup> animals were transfected or not (Control) with 10 μg/ml poly(I:C) for 4 h. During the activation, macrophages were treated or not with 5 mM GEE. IL-1β present in cellular supernatants was quantified with a specific ELISA.
- I Mice were treated with 1 mg/kg cyclosporine A for 1 h and then injected with 20 mg/kg of poly(I:C). Four hours later, serum was collected and IL-1β levels were analyzed with a specific ELISA.

Data information: Data shown (A–D, H) are from biological triplicate samples and are shown as mean ± SEM. Two independent experiments were performed. Data in (E–G) are from duplicate biological samples. (I) Data shown are from three Wt animals, and five *Lpin2*<sup>−/−</sup> animals treated with poly(I:C) and 4 Wt and *Lpin2*<sup>−/−</sup> animals treated with Cyclosporin A and poly(I:C). Data represent the mean ± SEM. \**P* < 0.05; \*\**P* < 0.01; \*\*\**P* < 0.001; #*P* < 0.05; ##*P* < 0.01; ###*P* < 0.001; &#P < 0.05; &&#P < 0.01, Student's *t*-test. \*, *Lpin2*-deficient vs. control cells/animals; #, Tr. poly(I:C) treated cells/animals vs. control cells/animals of the same phenotype; &, p<sup>0</sup> vs. cells of the same phenotype and activation.

Source data are available online for this figure.

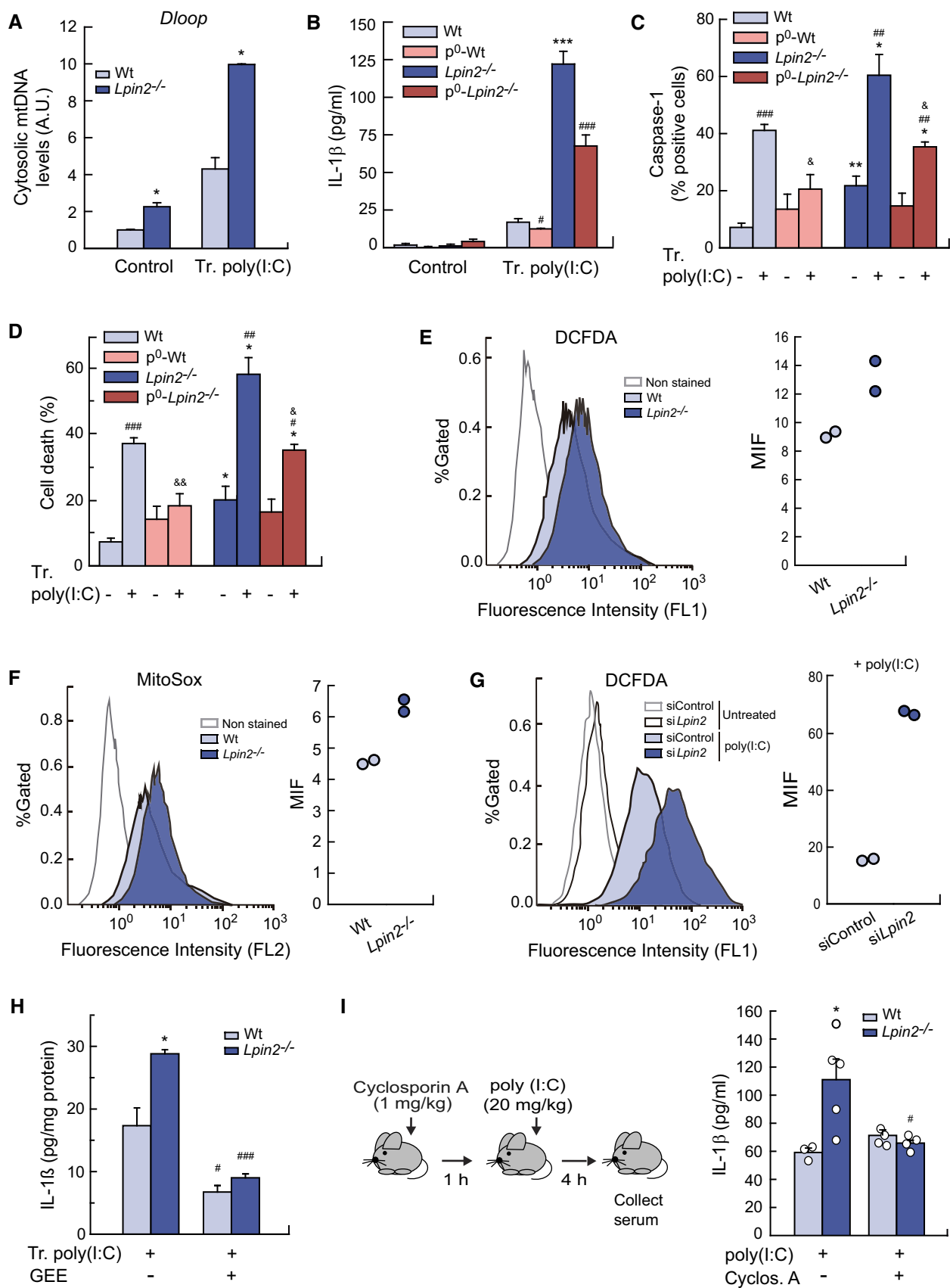


Figure 7.

eliminated mtDNA by treating immortalized wild type and *Lpin2*<sup>-/-</sup> BMDMs with ethidium bromide ( $\rho^0$  phenotype) (King & Attardi, 1989). IL-1 $\beta$  synthesis was then evaluated in primed macrophages transfected with poly(I:C). We found that elimination of mtDNA significantly reduced IL-1 $\beta$  production, and such reduction was more pronounced in cells deficient in lipin-2 (Fig 7B). In agreement with these data, we also observed that loss of mtDNA decreased the activation of caspase-1 by transfected poly(I:C) in both wild type and lipin-2-deficient cells, as analyzed by flow cytometry (Fig 7C). As a consequence, cell death was also decreased in  $\rho^0$  cells from both phenotypes (Fig 7D).

During NLRP3 inflammasome activation by mtDNA, oxidative processes appear to play an important role (Zhong et al, 2018). By using specific fluorescent probes, we measured total ROS production in cells and also specifically in mitochondria. We found that lipin-2-deficient cells transfected with poly(I:C) produced significantly more ROS, both total and mitochondrial, than cells expressing normal lipin-2 levels (Fig 7E and F). The same effect in cellular ROS production was observed upon extracellular poly(I:C) treatment (priming signal for inflammasome activation through TLR3) (Fig 7G). Interestingly, treatment of macrophages with the antioxidant glutathione ethyl ester (GEE) strongly blunted the production of IL-1 $\beta$ , an effect that was more marked in BMDMs from *Lpin2*<sup>-/-</sup> animals (Fig 7H).

One of the mechanisms that have been described for mtDNA exit from the mitochondria is through the opening of the mitochondrial permeability transition pore, which occurs during excessive ROS production (Rottenberg & Hoek, 2017; Bahat et al, 2021). Pore opening can be inhibited by cyclosporin A, a drug that has also been shown to destabilize mitochondria and reduce IL-1 $\beta$  production by a number of stimuli (Iyer et al, 2013). To evaluate whether the findings reported above could be relevant to animal models of inflammation, we analyzed IL-1 $\beta$  levels in the serum of animals treated with poly(I:C), and analyzed the effect of cyclosporin A pretreatment as well. We found that cyclosporin A severely curtailed IL-1 $\beta$  production in lipin-2-deficient animals, while having no discernible effect on wild type animals (Fig 7I).

Overall, these results suggest that lipin-2 restrains both mtDNA release and oxidative events that play a role during inflammasome activation by viral nucleic acid mimics.

### Lipin-2 controls IL-1 $\beta$ during cytomegalovirus infection

To corroborate our findings with poly(I:C) regarding IL-1 $\beta$  production, experiments were also conducted with MCMV-infected macrophages. We found that the absence of lipin-2 increased IL-1 $\beta$  levels in the supernatants of MCMV-infected BMDMs (Fig EV1A). Accordingly, virus-infected *Lpin2*<sup>-/-</sup> animals had higher concentrations of the cytokine in serum than control ones (Fig EV1B). The same behavior was also found in HCMV-infected human macrophages (Fig EV1C). These results confirm that lipin-2 restricts inflammasome activation during viral encounters.

### *LPIN2* expression decreases in symptomatic COVID-19 patients and correlates with increases in damaging factors

Late in 2019, a new coronavirus, SARS-CoV-2, was identified as the cause of a severe acute respiratory syndrome known as COVID-19

(Chen et al, 2020; Zhou et al, 2020). Although the majority of infected people are asymptomatic or develop mild symptoms, a significant number of patients develop a severe disease. As a consequence, around 1% of the patients die and some suffer from long-standing sequelae.

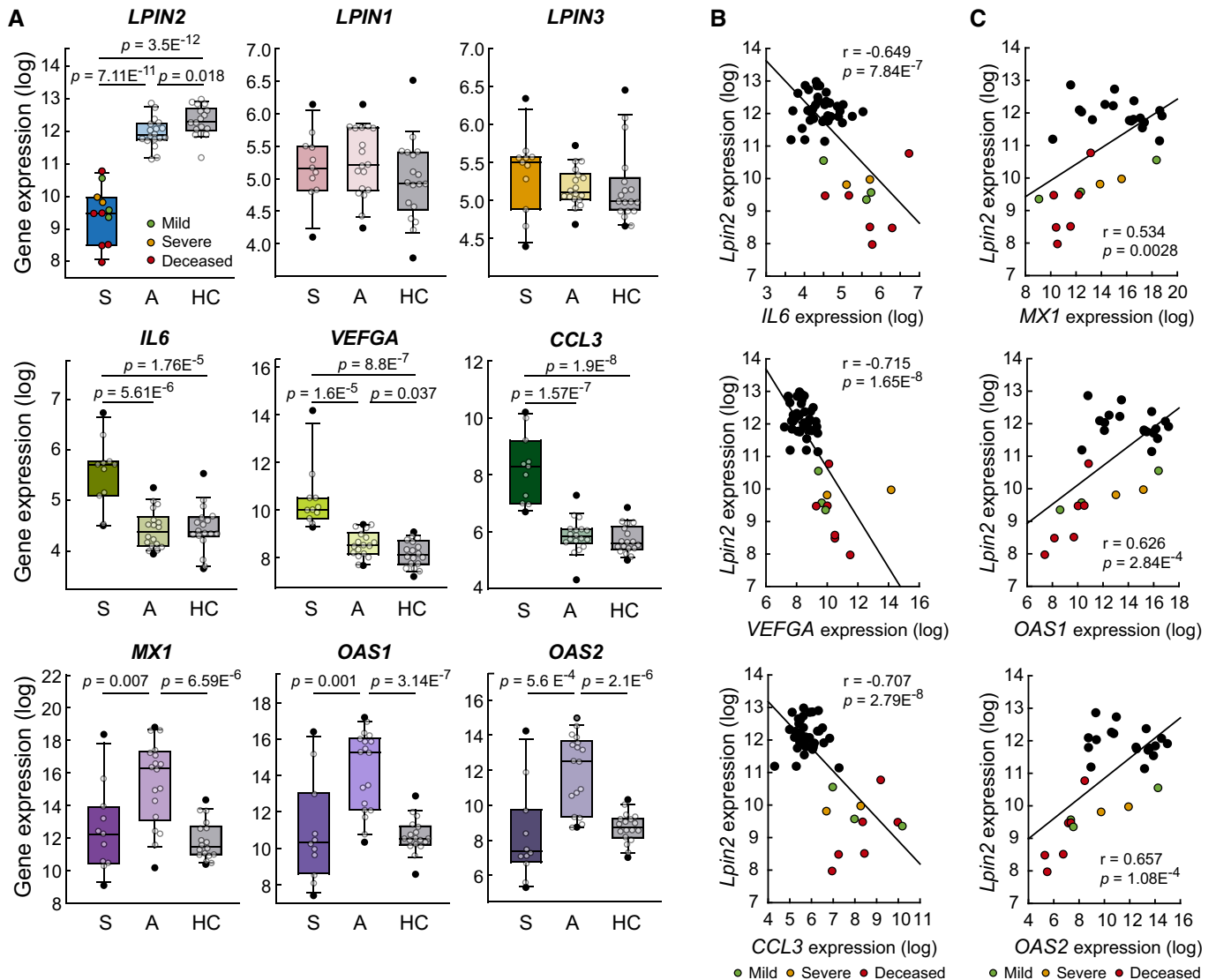
Severity of COVID-19 has been associated with a dysfunctional immune response characterized by low or delayed IFN responses and exaggerated production of proinflammatory cytokines (Hadjadj et al, 2020). An interesting feature of SARS-CoV-2 infection is that the virus modulates the immune response in a way that suppresses the IFN-I system but induces and sustains high levels of chemokine mRNAs, resulting in an imbalanced host response (Konno et al, 2020; Lei et al, 2020; Miorin et al, 2020; Thoms et al, 2020; Xia et al, 2020). Indeed, it has been demonstrated that upregulation of IFN responses in COVID-19 asymptomatic patients correlates with a better control of the illness (Masood et al, 2021a).

Based on the findings described above showing that lipin-2 levels are regulated by IFN and that the expression levels of lipin-2 inversely modulate the proinflammatory capacity of macrophages, we sought to analyze whether *LPIN2* levels were altered in COVID-19 patients. We analyzed public available databases of gene expression arrays from blood samples of healthy control subjects, asymptomatic and symptomatic patients (Masood et al, 2021a; Data ref: Masood et al, 2021b). The results are shown in Fig 8 and indicate that *LPIN2* levels were significantly decreased in symptomatic compared with asymptomatic individuals or healthy control subjects (Fig 8A). Interestingly, patients with lower expression of *LPIN2* experienced severe symptoms and were actually not able to recover from the illness (Fig 8A). The rest of the genes of the *LPIN* family, *LPIN1* and *LPIN3* showed no changes in their expression levels. As previously described, samples from symptomatic patients showed an increased expression of the proinflammatory genes *IL6*, *VEFGA* and *CCL3*, related with the cytokine storm (Chen et al, 2020), the endothelial dysfunction (Rovas et al, 2021), and the increased recruitment of innate immune cells (Chi et al, 2020) that characterize patients with severe COVID-19 (Masood et al, 2021a). Interestingly, *LPIN2* expression levels negatively correlated with the expression of these genes (Fig 8B). However, canonical ISGs such as *MX1*, *OAS1*, and *OAS2* showed higher expression levels in asymptomatic patients than in symptomatic ones, as shown for *LPIN2* (Fig 8A and C). Collectively, these results are highly suggestive of a correlation between *LPIN2* expression levels and IFN responses and the capacity to overcome the disease in COVID-19 patients.

## Discussion

After viral interference factors were discovered in the late 50's (Isaacs & Lindenmann, 1957), research on IFNs has demonstrated that they exert a myriad of effects on pathogen elimination, immunity and metabolism. To exert their actions, IFN receptors activate a complex array of transcription factors that participate in the regulated expression of many different genes. The identification and description of the roles of the proteins encoded by those genes is crucial to better define how IFNs impact on the aforementioned processes. Here we unveil the regulated expression of *Lpin2* by IFNs, and the involvement of this phosphatase in a number of key immunoinflammatory events. These include the control of viral infections,





**Figure 8. LPIN2 expression decreases in symptomatic COVID-19 patients.**

A–C Gene expression analyses were performed using the GSE177477 database. (A) Box plots showing the indicated gene expression analysis in samples from symptomatic (S,  $n = 11$ ) and asymptomatic (A,  $n = 18$ ) patients with COVID-19, and healthy controls (HC,  $n = 18$ ). The central band is the median, boxes define 25<sup>th</sup> to 75<sup>th</sup> percentiles and whiskers 10<sup>th</sup> and 90<sup>th</sup> percentiles.  $P$  as shown by Student's  $t$ -test. (B–C) Scatter plots showing the correlation between LPIN2 and proinflammatory/damage-related gene expression levels ( $n = 47$ , B), or between LPIN2 and canonical ISGs expression levels (COVID-19 samples,  $n = 29$ , C). Pearson's coefficient tests were performed to assess statistical significance.

Source data are available online for this figure.

inflammasome activation by viral-derived PAMPs, and the negative correlation between LPIN2 levels and severity of COVID-19.

Macrophages possess the ability to differentially reprogram their lipidome in response to TLR stimulation (Hsieh *et al*, 2020). In BMDMs, TLRs are able to modify the cellular levels of a number of lipid families, including phospholipids, DAG and TAG. Deletion of the IFN receptor *ifnar* results in reduced production of TAG (Hsieh *et al*, 2020). Together with our present results, these studies suggest a scenario whereby the capacity of certain TLRs to reprogram the lipidome in macrophages to generate TAG may depend on their capacity to generate IFN, and that lipin-2, a lipid phosphatase that participates in TAG synthesis, may act as master regulator of

the pathway. Of note, the other members of the lipin family, lipin-1 and lipin-3 are down regulated or very modestly regulated, respectively, during TLR or IFN stimulation of macrophages.

The finding that lipin-2 acts as an antiviral effector for MCMV infection is in agreement with its regulation by IFN, both being part of the mechanisms that the cytokine puts into motion to fight the viral infection. Several metabolism-related effects found during human cytomegalovirus infection could help to explain the antiviral role of lipin-2. In the first place, factors such as *Rsad2*/viperin, an ISG that is used as part of the IFN-induced antiviral response to inhibit the replication of many viruses, may be used by cytomegaloviruses in their own benefit to increase viral infectivity (Seo

et al, 2011; Dumbrepatil et al, 2020). The mechanism appears to be related with the relocation of viperin from the endoplasmic reticulum to mitochondria, where it inhibits  $\beta$ -oxidation and ATP production. This will result in disruption of the actin cytoskeleton, and also with the accumulation of lipids that the virus needs to form the viral envelope (Seo et al, 2011; Dumbrepatil et al, 2020). Interestingly, we show here that lipin-2 reduces *Rsad2*/viperin expression in macrophages during viral-derived PAMP activation, thus suggesting a possible metabolic mechanism to restrict cytomegalovirus replication. Second, it is well known that IFN reduces cholesterol synthesis to control viral infection (Blanc et al, 2011). However, it has also been described that human cytomegalovirus promotes cholesterol efflux from infected cells through viral proteins, thus helping the virus escape immune control (Low et al, 2016). In this regard, we have previously described that lipin-2 impacts on macrophage cholesterol levels in such a way that, in the absence of lipin-2, the levels of cholesterol are reduced in macrophages (Lordén et al, 2017). Thus, during an infection with cytomegalovirus, the effect that lipin-2 exerts on cholesterol levels could be disadvantageous for cytomegalovirus propagation and immune evasion.

Majeed syndrome patients that carry mutations in the *LPIN2* gene develop very early in their lives symptoms such as recurrent episodes of fever and inflammation in bones and skin (Majeed et al, 1989; Ferguson et al, 2005). Macrophages defective in *LPIN2* have an enhanced predisposition to activate the inflammasome NLRP3 in a classical way (Lordén et al, 2017). Interestingly, we have now discovered that viral-associated molecular patterns exhibit the capacity to both increase signaling during the priming step of inflammasome activation and promote an increased inflammasome activation when recognized intracellularly by macrophages. These findings may be important to explain, at least in part, why Majeed syndrome patients suffer from recurrent episodes of fever without obvious infection. It seems likely that low-load viral infections, which would not generate symptoms in healthy individuals, could induce the production of the pyrogen IL-1 $\beta$ , reaching levels high enough to generate peaks of fever in Majeed patients (Dinarello et al, 1986). Also, the exaggerated production of IL-1 $\beta$  by myeloid cells from these patients may influence the polarization of anti-inflammatory/regulatory macrophages (M2), to generate M2 cells that express proinflammatory cytokines such as IL-6 or TNF $\alpha$ , and display increased osteoclastogenic capacity (Bhuyan et al, 2021). The increased levels of IL-1 $\beta$  promoted by low levels of viral infections could participate in the development of proinflammatory M2 macrophages. This would provide an explanation to the flares of osteomyelitis that these patients also develop.

Our results related with the mechanism through which intracellular viral nucleic acid mimics increase inflammasome activation in lipin-2-deficient macrophages, prompt us to consider that, similar to what we have observed in lipin-2-deficient mice, treatment of patients with inhibitors of mtDNA release may help reduce inflammasome activation during viral encounters. This would lower IL-1 $\beta$  synthesis and ameliorate symptoms in these patients. One of these inhibitors, cyclosporin A, has been used in the clinic as an immunosuppressant during organ transplantation for decades. Due to the recent confirmation of the importance of the mitochondrial permeability transition pore in the development of many diseases, inhibitors such as cyclosporine A have now been proposed as possible

treatment options for these conditions, including viral infections (Winqvist & Gribkoff, 2020; Han et al, 2022).

Despite the detrimental actions of an excessive and uncontrolled IL-1 $\beta$  production, the importance of inflammasomes and IL-1 $\beta$  in antimicrobial defenses is demonstrated by the increased susceptibility to infections exhibited by mice and humans defective in IL-1 $\beta$  receptor/inflammasomes (Man et al, 2017). It is manifested as well by the capacity of viruses and other pathogens to dampen the production and actions of the cytokine (Biolatti et al, 2018). Thus, it is tempting to speculate that a consequence of the enhanced inflammasome activation in Majeed syndrome patients would also include a more effective elimination of some viruses that are very sensitive to inflammasome activation. However, we also show in this work that viruses that developed robust mechanisms to evade innate immune responses such as cytomegaloviruses (Biolatti et al, 2018), are able to replicate better in the absence of lipin-2. Infection of Majeed syndrome patients with this type of viruses would predictably be more severe. In this regard, the conclusions obtained from samples from SARS-CoV-2-infected patients point to the idea that patients with *LPIN2* mutations and/or reduced *LPIN2* expression levels would be at risk for severe COVID-19. Overall, it may seem that, depending on the type of virus, Majeed syndrome patients would be more protected, or more vulnerable to infection. Either case, they would presumably display an exacerbated inflammasome activation and IL-1 $\beta$  production during the encounters.

In the current COVID-19 pandemic only a minor portion of the patients develop a severe disease and eventually die. Most of the population is believed to be able to mount an early and strong antiviral, IFN-dependent response that reduces viral replication and spreading from the upper airways to the lungs and other tissues (Blanco-Melo et al, 2020). If initial IFN responses are defective, SARS-CoV-2 replicates without control, spread to the abovementioned organs, and inflammation exacerbates due to an exaggerated immune cell recruitment (Zhang et al, 2020a). These antiviral actions occur in spite of the SARS-CoV-2 capacity to decrease IFN responses (Xu et al, 2021). Thus it is important to identify in the very early steps of infection those patients who could have difficulties to mount an adequate antiviral response. We have identified that *LPIN2* expression levels in blood samples from Covid-19 patients provide a clear-cut difference between symptomatic from asymptomatic patients. *LPIN2* levels appear to perform better in this regard than canonical ISGs like *MX1*, *OAS1* or *OAS2*. Whether the low levels of *LPIN2* in symptomatic Covid-19 patients are a cause or a consequence of the disease, cannot be told at this stage. We speculate that patients with constitutive low *LPIN2* expression levels could be at risk of experiencing a more severe disease due to the increased inflammatory response. This idea receives support from the fact that expression levels of inflammatory and damage-related factors such as *IL6*, *VEFGA* and *CCL3* inversely correlate with *LPIN2* expression. However, based on our observations that *LPIN2* expression is regulated by IFNs, it is also possible that *LPIN2* levels in COVID-19 patients reflect their IFN responses.

Whatever the cause for the reduced levels of *LPIN2* in symptomatic patients, we are tempted to speculate that early analysis of *LPIN2* expression in COVID-19 patients could help in the stratification of those patients. Those with very low *LPIN2* levels would possibly develop a severe illness; hence they could benefit from early treatment with exogenous IFN, more specifically, IFN- $\beta$  (Vinh

*et al.*, 2021; Sodeifian *et al.*, 2022). This treatment has proven to be efficacious in critical COVID-19 patients with inborn errors for IFN or that carry autoantibodies against IFN (Bastard *et al.*, 2020; Zhang *et al.*, 2020b, 2022; Aricò *et al.*, 2022). Clearly, future studies should validate *LPIN2* as an accurate biomarker of IFN action and/or COVID-19 severity, and its use for the design of personalized therapies.

## Materials and Methods

### Reagents

LPS (*Escherichia coli* 0111: B4), and poly(I:C) (P0913) were from Sigma-Aldrich. N-palmitoyl-S-[2,3-bis(palmitoyloxy)-(2R,2S)-propyl]-Cys-[S]-Ser-[S]-Lys(4) trihydrochloride (Pam3SCK4), lipoteichoic acid from *Staphylococcus aureus* (LTA), S-(2,3-bis(palmitoyloxypropyl)-Cys-Gly-Asp-ProLys-His-Pro-Ser-Phe (FSL-1), imiquimod, and synthetic oligodeoxynucleotide 1826 (5-TCCATGACGTTCTGACGTT-3; ODN1826) were purchased from InvivoGen. Murine IFN- $\beta$  (12405-1) was from Pbl Assay Science, and murine IFN- $\gamma$  (12343534) was from Immunotools. Actinomycin D (294940010), cycloheximide (AC357420010), and cyclosporine A (457970010) were purchased from Thermo Scientific. The antibody against lipin-2 was obtained from Bethyl Laboratories (A303-703A) (Montgomery, TX, USA). Antibodies against phospho-p38 MAPK (Thr180/Tyr182) (4511), phospho-p44/42 MAPK (p-ERK) (Thr202/Tyr204) (9101), phospho-SAPK/JNK (Thr183/Tyr185) (4668), p38 MAPK (9212), p42-p44 MAPK (ERK) (4695), SAPK/JNK (9252), NF-KB p65 (8242) and IL-1 $\beta$  (12242) were from Cell Signaling. Antibodies against active caspase-1 (sc-515) were from Santa Cruz. Nigericine, Ac-YVAD-AOM, and SB203582 were from Calbiochem, Ruxolitinib was from LC Laboratories. Specific kits for the measurement of IL-1 $\beta$  and IL-18 levels were from Invivogen (#88-7013-88) and Sino Biologicals (#E-EL-M0033), respectively. All other reagents were purchased from Sigma-Aldrich.

### Animals

Mice, including *Lpin2*<sup>-/-</sup> animals, were maintained as previously described (Lordén *et al.*, 2017). 8–12-week-old animals were used for experimentation in sex-matched groups. Wild type littermates were used as control animals (heterozygous animals were used for breeding). All procedures involving animals were carried out under the supervision of the Institutional Committee of Animal Care and Usage of the University of Valladolid (Approval No. 7406000), and are in accordance with the guidelines established by the Spanish Ministry of Agriculture, Food, and Environment, and the European Union.

### Cells

Bone marrow-derived macrophages (BMDMs), primary human macrophages, and RAW264.7 cells were obtained, cultured, maintained and silenced as previously described (Valdearcos *et al.*, 2012; Rubio *et al.*, 2015; Lordén *et al.*, 2017). BMDMs were differentiated from precursors obtained from mice femurs by culturing for 7 days in RPMI 1640 supplemented with 10% FBS, 20% conditioned media from L929 fibroblast, 100 U/ml penicillin, and 100  $\mu$ g/ml streptomycin.

Human macrophages were differentiated from human blood monocytes present in buffy coats of healthy anonymous volunteer donors obtained from the Centro de Hemoterapia y Hemodonación de Castilla y León (Valladolid, Spain), as previously described (Rubio *et al.*, 2015; Lordén *et al.*, 2017). Blood cells were diluted with PBS (1:1), layered over a cushion of Ficoll-Paque and centrifuged at 750 g for 30 min. Mononuclear cells from the interphase were collected, washed with PBS, resuspended in RPMI 1640 free of serum and allowed to adhere to sterile plastic dishes for 2 h at 37°C. Non-adherent cells were extensively washed out. Macrophage differentiation was achieved by incubating adherent monocytes in RPMI with 5% of human serum (which contains high quantities of M-CSF) in the absence of other cytokine sources for 10–14 days. Culture medium was replaced every 3 days.

RAW 264.7 macrophages (ATTC, TIB-71<sup>TM</sup>) were cultured in DMEM supplemented with 10% FBS, 100 U/ml penicillin, 100  $\mu$ g/ml streptomycin, and 2 mM glutamine. MEFs derived from BALB/c mice were cultivated in DMEM supplemented 10% fetal bovine serum (FBS), 1 mM sodium pyruvate, 50 U/ml penicillin, 50  $\mu$ g/ml streptomycin, and 2 mM glutamine.

All cells were maintained under mycoplasma-free conditions. For inflammasome activation analyses, cells were primed with 10 ng/ml of poly(I:C) for 4 h. Afterward, they were transfected with 10 ng/ml poly(I:C) using 0.8  $\mu$ l Lipofectamine (Thermo Fisher Scientific) per mg poly(I:C) for 4 h.

### Gene silencing

Gene expression silencing was performed in murine cells using specific ON-Target plus siRNAs obtained from Dharmacon (Thermo Scientific). Control siRNAs were ON-Target plus Non-targeting Control Pool siRNAs (D-00810-10). BMDMs and RAW 264.7 cells were silenced by introducing complexes of siRNAs (20 nM final concentration in culture) with Lipofectamine RNAiMAX (Thermo Fisher Scientific) as specified by the manufacturer (Pindado *et al.*, 2007; Ruipérez *et al.*, 2009). The cells were used after 2 days of transfection.

For *LPIN2* silencing in human cells Silencer<sup>®</sup> Select siRNAs were obtained from Ambion (sense sequence, 5'-GAA GUU GGG UGA UAA CGG ATT-3', and antisense sequence 5'-UCC GUU AUC ACC CAA CUU CAT-3'). Control siRNAs used were Ambion<sup>™</sup> Silencer<sup>™</sup> Select Negative Control No.2 siRNAs (4390847). siRNAs were introduced after 10–14-days differentiation by Nucleofection (Amaxa Biosystems) following the manufacturer's instructions (Y-010 program), at 20–40 nM siRNA final concentration in culture (Valdearcos *et al.*, 2011). Macrophages were placed in culture and allowed to rest for 2 days. A 75–90% reduction of lipin-2 levels was routinely achieved using this methodology.

### Immunoblot

Cell homogenates were obtained by lysis with the buffer 20 mM Tris pH 7.4, 150 mM NaCl, 1 mM EDTA, 1 mM EGTA, 5 mM Na<sub>4</sub>P<sub>2</sub>O<sub>7</sub>, 50 mM  $\beta$ -glycerophosphate, 270 mM sucrose, 0.1% 2-mercaptoethanol, 1% Triton X-100, 100  $\mu$ M PMSF, 1 mM Na<sub>3</sub>VO<sub>4</sub>, 10 mM NaF and a protease inhibitor cocktail (P-8340, Sigma). After centrifugation at 15,000 g for 10 min, 50–100  $\mu$ g of cellular protein was separated by SDS-PAGE and transferred to PVDF membranes.

Blocked membranes (5% defatted dry milk or 5% bovine serum albumin in PBS) were then treated with specific antibodies at 1:1,000 in PBS with 0.5% defatted dry milk and 0.1% Tween 20. The exception was anti-lipin-2 (1:500) and  $\beta$ -actin (1:20,000). Secondary antibodies HRP linked (GE Healthcare #NA931 and #NA9340) were used at 1:5,000 dilution. Bands were visualized using ECL chemiluminescent substrate (Amersham Biosciences).

For analysis of protein present in cellular supernatants, trichloroacetic acid was added to supernatants at a final concentration of 10%, mixed vigorously and incubated at 4°C for 30 min. Samples were then centrifuged at 16,000 g 10 min at 4°C. Pellets were washed with cold acetone, dried at 63°C, resuspended in PBS and analyzed by immunoblot.

### Quantitative PCR (qPCR)

RNA was obtained using the TRIzol reagent (Ambion) and cDNA was then produced using Verso cDNA Synthesis Kit (Thermo Fisher Scientific), following the manufacturer's instructions. qPCR was performed from 20 ng of cDNA using the Brilliant III Ultra-Fast SYBR® Green QPCR Master Mix (Agilent Technologies), following the manufacturer's instructions. Relative mRNA expression was obtained using the  $\Delta\Delta C_t$  method (Schmittgen & Livak, 2008). Quantitative real-time RT-PCR analysis was performed in a LightCycler 480 (Roche) as previously described (Valdearcos et al, 2012; Meana et al, 2014). Genes of reference were *Gapdh* for murine cells, and *ACTB* for human cells. Primers used for murine genes were: *Gapdh* AGGTCGGTGTGAACGGATTG and TGTAGACCATGTAGTTGAGG TCA; *Lpin1*, CTCCGCTCCCAGAGAAAAG and TCATGTGCAAATCC ACGGACT; *Lpin2*, AGTTGACCCATCACCGTAG and CCCAAAGCA TCAGACTTGGT; *Lpin3*, TGGAATTGGGATGACAAGGT and CAC TGCAAGTACCCCTTGGT; *Il1b*, GCAACTGTTCCCTGAACCTCACT and TCTTTTGGGGTCCGTCAACT; *Il18*, CAAACCTTCAAATCACTT CCT and TCCTTGAAGTTGACGCAAGA; *Irf7*, GAGACTGGCTATT GGGGAG and GACCGAAATGCTTCCAGGG; *Nlrp3*, ATCAACA GGCGAGACCTCTG and GTCCTCCTGGCATAACATAG; *Rsd2*, TG CTGGCTGAGAATAGCATTAGG and GCTGAGTGCTGTCCCATCT; *Tlr3* GTGAGATAACAACGTAGCTGACTG and TCCTGCATCCAAG ATAGCAAGT; *Ifih1* AGATCAACACCTGTGGTAACACC and CTCTA GGGCCTCCAGGAACA; *Eif2k2* ATGCACGGAGTAGCATTACG and TGACAATCCACTTGTTTTCG T; *Ddx58* AAGAGCCAGAGTGTC AGAATCT and AGCTCCAGTTGGTAATTTCTTGG. Primers used for human genes were: *ACTB*, ATTGCCGACAGGATGCAGAA and GC TGATCCACATCTGCTGGAA; *LPIN2*, CCTCTCCTCAGACCAGATCG and GGAGAATCTGTCCCAAAGCA; *IL1B*, ATGATGGCTTATTACAG TGGCAA and GTCGGAGATTCTGAGCTGGA.

### Constructs

The plasmid mlipin-2-EGFP was previously described (Valdearcos et al, 2012). A plasmid expressing only lipin2 was generated by introducing of a stop codon between the lipin-2 and EGFP sequences using the Q5 site-directed mutagenesis Kit (New England Biolabs). The primers used were: 5'-aagtcgacggtaccgcgggcCCCGGGATC-CATCG-3' and 5'-aagccaggtatccaggtcATTGGG TCTCGCCAG-3'. Confirmation of the correct insertion of the cDNA was performed by sequencing. Plasmids were transfected using Lipofectamine™ LTX and PLUS™ reagents following the manufacturer's instructions.

### Microarray expression data

To study the kinetics of mRNA expression levels of BMDMs treated with either LPS (0.5 ng/ml, 5 ng/ml, or 50 ng/ml), or IFN- $\beta$  or IFN- $\gamma$  (10 U/ml), data were obtained from GSE44292 and analyzed as previously described (Raza et al, 2014a; Data ref: Raza et al, 2014b).

Gene expression data of MCMV infected BMDMs was obtained from GSE42505 and analyzed as previously described (Blanc et al, 2013; Data ref: Blanc et al, 2015). Data to unravel the participation of STAT1 in gene expression induced by treatment of BMDMs (wild type and *Stat1*<sup>-/-</sup>) with 100 U/ml IFN- $\gamma$  for 6 h were obtained from GSE48970 and analyzed as previously described (Semper et al, 2014a; Data ref: Semper et al, 2014b).

### Newly transcribed mRNA

Newly transcribed *Lpin2* mRNA data were obtained from GSE63290. Experimental design and data analysis was described elsewhere (Dölken et al, 2008; Robertson et al, 2016; Data ref: Robertson & Ghazal, 2016). Briefly, BMDMs were left untreated or treated with 10 U/ml IFN- $\gamma$ . Newly transcribed RNA was then labeled with 200  $\mu$ M 4-thiouridine every 30 min for 8 h. For analysis, newly transcribed RNA samples and total RNA samples were hybridized to Affymetrix GeneST v1.0 arrays.

### Chip-seq analysis of STAT1 binding to *Lpin2* locus

Data from Chip-Seq experimentation using BMDMs stimulated with IFN- $\beta$  or IFN- $\gamma$  for 6 h were obtained from GSE33913. The experimental details were described elsewhere (Ng et al, 2011a; Data ref: Ng et al, 2011b). Briefly, chromatin from stimulated cells was cross-linked and immunoprecipitated using antibodies against STAT1 (Santa Cruz). After sequencing, STAT1 peaks were defined using Model-based analysis of ChIP-Seq (MACS) (Zhang et al, 2008). Reads were aligned to the mouse genome and normalized to reads per kilobase per million reads sequenced (RPKM) (Ng et al, 2011a; Data ref: Ng et al, 2011b).

### In vitro viral infection

For *in vitro* infection experiments, the MCMV-GFP recombinant virus, a derivative of the BAC MCMV MW97.01 based on the MCMV strain (ATCC VR-1399) that carries the GFP gene inserted in the *ie2* locus, was used (Mathys et al, 2003). Macrophages were infected with MCMV-GFP at 2–4 multiplicity of infection (MOI) during 2 h, including a centrifugal enhancement of infectivity step (Hudson, 1988). Cells were then washed with PBS and fresh culture medium was added. GFP fluorescence of the cell cultures was analyzed after infection using a Fluoroskan Ascent FL Fluorimeter (Thermo Electron Corporation) employing a wavelength of 475 nm for fluorescence excitation and 510 nm for fluorescence emission. For experiments with human macrophages, the HCMV strain TB40/E was used (Sinzger et al, 2008).

To quantify infectious virus, supernatants from infected macrophages were harvested, clarified, and transferred to MEFs immortalized by p53 to determine by standard plaque assay titrations viral plaque-forming units (PFU) or fluorescence-forming units (FFU) using a fluorescence microscope.



IL-1 $\beta$  production was measured using BMDMs or human macrophages primed with 200 ng/ml of LPS before MCMV (MOI = 2) or HCMV infection (MOI = 5) respectively. Cell supernatants were obtained 36 h after infection, and analyzed for IL-1 $\beta$  content by ELISA.

#### **In vivo viral infection model**

For *in vivo* viral infections, the BAC-derived MCMV MW97.01, referred here as MCMV, was used (Wagner *et al*, 1999). Mice were intraperitoneally infected with 1 ml PBS containing  $3.5 \times 10^6$  PFU of MCMV. After 5 days of infection, mice were anesthetized with 100 mg/kg ketamine (Merial) and 5 mg/kg xylazine (Bayer). Mice were sacrificed by cervical dislocation to harvest the organs of interest. Livers and spleens were homogenized in DMEM 3% FBS (10% weight/volume), sonicated, centrifuged and viral titers from the supernatants were determined by standard plaque assays, including a centrifugal enhancement step, following the same protocol mentioned above. For IL-1 $\beta$  quantification, mice were infected for 36 h. Afterward, serum was collected and IL-1 $\beta$  was analyzed by ELISA.

#### **In vivo inflammasome activation model**

Mice were intraperitoneally treated with 1 mg/kg cyclosporin A for 1 h to inhibit the mitochondrial permeability transition pore, and then injected with 20 mg/kg poly(I:C) to induce inflammasome activation. After 4 h of treatment, serum was collected as described above. Serum concentration of IL-1 $\beta$  was analyzed by ELISA.

#### **Immunostainings**

Cells were seeded in glass coverslips, stimulated and washed before they were fixated with 4% PFA and 3% sucrose 10 min at room temperature. Cells were permeabilized with 0.1% Triton X-100 for 2 min, washed three times with PBS, and incubated in 0.5% BSA, 50 mM glycine, and 4% goat serum in PBS for 30 min at room temperature. Cells were then washed three times and incubated with an anti-p65 antibody (1:200) (Cell Signaling), diluted in 0.1% BSA (w/v) in PBS for 1 h at room temperature. After washing, cells were incubated with an Alexa Fluor®488-goat anti rabbit (1:2,000) diluted in 0.1% BSA (w/v) in PBS for 1 h at room temperature, protected from light. Finally, nuclei were stained with 1  $\mu$ g/ml DAPI in PBS for 5 min at room temperature, and washed with milli-Q H<sub>2</sub>O. Coverslips were mounted onto slides and fluorescence was examined using an oil immersion, 63 $\times$ , 1.4 NA, HCX PL APO CS objective in a Leica TCS SP5X confocal microscope. DAPI was excited using an UV laser line at 405 nm and fluorescence emission was collected between 441 and 470 nm. AF®488 was excited using a supercontinuum visible laser, at 488 nm and fluorescence emission was collected between 499 and 545 nm. To obtain the percentage of cells with p65 in the nucleus, all the nuclei in the image (DAPI) and the nuclei with green staining (p65) were counted using the Cell Counter plugin of ImageJ.

#### **Flow cytometry**

Active caspase-1 was assayed using the probe FAM-FLICA (FAM-YVAD-FMK, Immunochemistry Technologies), a fluorescent

inhibitor that binds and labels active caspase-1. The manufacturer's instructions were followed. Briefly, the cells were labeled with FAM-FLICA during 1 h at 37°C, washed to eliminate the excess of probe, and fluorescence was analyzed by flow cytometry (FL1, Gallios, Beckman Coulter). Data analysis was performed using the software Kaluza, version 1.3.

Cellular membrane permeabilization was assayed by PI uptake. Briefly, cells were treated with 50  $\mu$ g/ml of PI in PBS for 5 min, and cellular fluorescence analyzed by flow cytometry in FL3. Data was analyzed using the Kaluza software.

To measure total cellular ROS or mitochondrial ROS levels, the probe DCFDA (2',7'-dichlorofluorescein diacetate, Sigma-Aldrich) or MitoSOX were used respectively. Briefly, cells were stimulated and treated with 10  $\mu$ M DCFDA or 5  $\mu$ M MitoSOX during the last 30 min of stimulation. Cells were then washed twice with PBS and fluorescence analyzed by flow cytometry (FL1 for DCFDA, or FL2 for MitoSOX, Gallios, Beckman Coulter). Data analysis was performed using the software Kaluza, version 1.3.

#### **MtDNA depletion**

Bone marrow-derived macrophages were cultured for 3 weeks in the presence of 100 ng/ml ethidium bromide, 100  $\mu$ g/ml sodium pyruvate and 50  $\mu$ g/ml uridine, as previously described (Nakahira *et al*, 2011). mtDNA depletion ( $\rho^0$ ) was confirmed by qPCR using primers for mitochondrial (*Dloop*) and nuclear (*Tert*) genes.

#### **Cytosolic mtDNA quantification**

Cytosolic mtDNA isolation and quantification was performed as previously described with slight modifications (West *et al*, 2015). Cells were divided into two equal aliquots. One aliquot was resuspended in Tri-reagent® (Molecular Research Center, Inc) to isolate total cellular DNA. These extracts were used as normalization controls for total mtDNA. Cells from the second aliquot were resuspended in 150 mM NaCl, 50 mM HEPES pH7.4, containing 20  $\mu$ g/ml digitonin to permeabilize the plasma membrane without disrupting the nucleus or any organelle. After 10 min incubation, the cells were centrifuged at 980 g for 3 min three times to obtain a cytosolic supernatant. This fraction was centrifuged further at 17,000 g for 10 min to completely eliminate nuclei, mitochondria, or endoplasmic reticulum. Protein was quantified from a small fraction and DNA was isolated from this cytosolic pure fractions using QIAquick Nucleotide Removal Columns (QIAGEN) following the manufacturer's instructions. A cytosolic volume equivalent to 1  $\mu$ g protein was used to analyze mtDNA content by qPCR using primers for *Dloop*. Ct values for *total Dloop* expression in total cellular DNA extract were used for normalization.

#### **Statistics**

No blinding of the data was performed. Except where indicated, data are described as means  $\pm$  standard error of the mean (SEM). Statistical significance was determined by Student's *t*-test, and one-way ANOVA followed by Holm-Sidak test conducted in SigmaPlot software, version 14.0.  $P < 0.05$  was considered statistically significant. Statistical tests and number of samples are described in the figure legends.



## Data availability

This study includes no data deposited in external repositories.

**Expanded View** for this article is available [online](#).

## Acknowledgements

We acknowledge support of the publication fee by the CSIC Open Access Publication Support Initiative through its Unit of Information Resources for Research (URICI). We thank Montserrat Duque and Eva Merino for technical assistance. This work was supported by the Spanish Ministry of Economy, Industry, and Competitiveness (grant SAF2016-80883-R), Spanish Ministry of Science and Innovation (MICIN/AEI/10.13039/501100011033; grants PID2019-105989RB-I00; PID2020-116918RB-I00; and PID2020-117425RB-C21), CIBERDEM-ISCI (grant CB07/08/0004), and the Regional Government of Castile and Leon (grant CSI141P20, cofinanced by the European Union through the European Regional Development Fund, "A Way of Making Europe"). N. de Pablo and J. Martínez-García were supported by predoctoral fellowships from the Spanish Ministry of Science and Innovation (FPU14-02879) and the Regional Government of Castile and Leon (E-47-2021-0015435), respectively. Instituto de Biología y Genética Molecular is a research center partnered between the Spanish National Research Council (CSIC) and the University of Valladolid.

## Author contributions

**Nagore de Pablo:** Data curation; formal analysis; investigation; methodology.

**Clara Meana:** Data curation; formal analysis; investigation; methodology.

**Javier Martínez-García:** Data curation; formal analysis; investigation;

methodology. **Pablo Martínez-Vicente:** Data curation; formal analysis;

investigation; methodology. **Manuel Albert:** Data curation; formal

analysis; investigation; methodology. **Susana Guerra:** Data curation; formal

analysis; supervision; funding acquisition; validation. **Ana Angulo:** Data

curation; formal analysis; supervision; funding acquisition; validation; writing

– original draft. **Jesús Balsinde:** Resources; formal analysis; supervision;

funding acquisition; validation; writing – original draft; project administration;

writing – review and editing. **María A Balboa:** Conceptualization; resources;

data curation; formal analysis; supervision; funding acquisition; validation;

visualization; writing – original draft; project administration; writing – review

and editing.

## Disclosure and competing interest statement

The authors state they have no competing interests or disclosures.

## References

- Aricò E, Bracci L, Castiello L, Urbani F, Casanova JL, Belardelli F (2022) Exploiting natural antiviral immunity for the control of pandemics: lessons from Covid-19. *Cytokine Growth Factor Rev* 63: 23–33
- Bahat A, MacVicar T, Langer T (2021) Metabolism and innate immunity meet at the mitochondria. *Front Cell Dev Biol* 9: 720490
- Balboa MA, Balsinde J, Dennis EA (1998) Involvement of phosphatidate phosphohydrolase in arachidonic acid mobilization in human amniotic WISH cells. *J Biol Chem* 273: 7684–7690
- Balboa MA, de Pablo N, Meana C, Balsinde J (2019) The role of lipins in innate immunity and inflammation. *Biochim Biophys Acta* 1864: 1328–1337
- Bastard P, Rosen LB, Zhang Q, Michailidis E, Hoffmann HH, Zhang Y, Dorgham K, Philippot Q, Rosain J, Béziat V et al (2020) Autoantibodies against type I IFNs in patients with life-threatening COVID-19. *Science* 370: eabd4585
- Bauernfeind FG, Horvath G, Stutz A, Alnemri ES, MacDonald K, Speert D, Fernandes-Alnemri T, Wu J, Monks BG, Fitzgerald KA et al (2009) NF- $\kappa$ B activating pattern recognition and cytokine receptors license NLRP3 inflammasome activation by regulating NLRP3 expression. *J Immunol* 183: 787–791
- Bhuyan F, de Jesus AA, Mitchell J, Leikina E, VanTries R, Herzog R, Onel KB, Oler A, Montealegre Sanchez GA, Johnson KA et al (2021) Novel Majeed syndrome-causing LPIN2 mutations link bone inflammation to inflammatory M2 macrophages and accelerated osteoclastogenesis. *Arthritis Rheumatol* 73: 1021–1032
- Biolatti M, Gugliesi F, Dell'Oste V, Landolfo S (2018) Modulation of the innate immune response by human cytomegalovirus. *Infect Genet Evol* 64: 105–114
- Blanc M, Hsieh WY, Robertson KA, Watterson S, Shui G, Lacaze P, Khondoker M, Dickinson P, Sing G, Rodríguez-Martín S et al (2011) Host defense against viral infection involves interferon mediated down-regulation of sterol biosynthesis. *PLoS Biol* 9: e1000598
- Blanc M, Hsieh WY, Robertson KA, Kropp KA, Forster T, Shui G, Lacaze P, Watterson S, Griffiths SJ, Spann NJ et al (2013) The transcription factor STAT-1 couples macrophage synthesis of 25-hydroxycholesterol to the interferon antiviral response. *Immunity* 38: 106–118
- Blanc M, Hsieh WY, Robertson KA, Kropp KA, Forster T, Shui G, Lacaze P, Watterson S, Griffiths SJ, Spann NJ et al (2015) Gene Expression Omnibus GSE42505. (<https://www.ncbi.nlm.nih.gov/geo/query/acc.cgi?acc=GSE42505>). [DATASET]
- Blanco-Melo D, Nilsson-Payant BE, Liu WC, Uhl S, Hoagland D, Møller R, Jordan TX, Oishi K, Panis M, Sachs D et al (2020) Imbalanced host response to SARS-CoV-2 drives development of COVID-19. *Cell* 181: 1036–1045
- Chen G, Wu D, Guo W, Cao Y, Huang D, Wang H, Wang T, Zhang X, Chen H, Yu H et al (2020) Clinical and immunological features of severe and moderate coronavirus disease 2019. *J Clin Invest* 130: 2620–2629
- Chi Y, Ge Y, Wu B, Zhang W, Wu T, Wen T, Liu J, Guo X, Huang C, Jiao Y et al (2020) Serum cytokine and chemokine profile in relation to the severity of coronavirus disease 2019 in China. *J Infect Dis* 222: 746–754
- Chow J, Franz KM, Kagan JC (2015) PRRs are watching you: localization of innate sensing and signaling regulators. *Virology* 479–480: 104–109
- Darnell JE Jr, Kerr IM, Stark GR (1994) Jak-STAT pathways and transcriptional activation in response to IFNs and other extracellular signaling proteins. *Science* 264: 1415–1421
- Decker T, Lew DJ, Mirkovitch J, Darnell JE Jr (1991) Cytoplasmic activation of GAF, an IFN-gamma-regulated DNA-binding factor. *EMBO J* 10: 927–932
- Dinarello CA, Cannon JG, Mier JW, Bernheim HA, LoPreste G, Lynn DL, Love RN, Webb AC, Auron PE, Reuben RC et al (1986) Multiple biological activities of human recombinant interleukin 1. *J Clin Invest* 77: 1734–1739
- Dölken L, Ruzsics Z, Rädle B, Friedel CC, Zimmer R, Mages J, Hoffmann R, Dickinson P, Forster T, Ghazal P et al (2008) High-resolution gene expression profiling for simultaneous kinetic parameter analysis of RNA synthesis and decay. *RNA* 14: 1959–1972
- Dumbrepatil AB, Zegalia KA, Sajja K, Kennedy RT, Marsh ENG (2020) Targeting viperin to the mitochondrion inhibits the thiolase activity of the trifunctional enzyme complex. *J Biol Chem* 295: 2839–2849
- Eaton JM, Takkellapati S, Lawrence RT, McQueeney KE, Boroda S, Mullins GR, Sherwood SG, Finck BN, Villén J, Harris TE (2014) Lipin 2 binds

- phosphatidic acid by the electrostatic hydrogen bond switch mechanism independent of phosphorylation. *J Biol Chem* 289: 18055–18066
- Ferguson PJ, El-Shanti H (2021) Majeed Syndrome: a review of the clinical, genetic and immunologic features. *Biomolecules* 11: 367
- Ferguson PJ, Chen S, Tayeh MK, Ochoa L, Leal SM, Pelet A, Munnich A, Lyonnet S, Majeed HA, El-Shanti H (2005) Homozygous mutations in *LPIN2* are responsible for the syndrome of chronic recurrent multifocal osteomyelitis and congenital dyserythropoietic anaemia (Majeed syndrome). *J Med Genet* 42: 551–557
- Franchi L, Eigenbrod T, Núñez G (2009) TNF- mediates sensitization to ATP and silica via the NLRP3 inflammasome in the absence of microbial stimulation. *J Immunol* 183: 792–796
- Gu Y, Kuida K, Tsutsui H, Ku G, Hsiao K, Fleming MA, Hayashi N, Higashino K, Okamura H, Nakanishi K et al (1997) Activation of interferon-gamma inducing factor mediated by interleukin-1 $\beta$  converting enzyme. *Science* 275: 206–209
- Hadjadj J, Yatim N, Barnabei L, Corneau A, Boussier J, Smith N, Péré H, Charbit B, Bondet V, Chenevier-Gobeaux C et al (2020) Impaired type I interferon activity and inflammatory responses in severe COVID-19 patients. *Science* 369: 718–724
- Han J, Lee MK, Jang Y, Cho WJ, Kim M (2022) Repurposing of cyclophilin A inhibitors as broad-spectrum antiviral agents. *Drug Discov Today* 27: 1895–1912
- Hsieh WY, Zhou QD, York AG, Williams KJ, Scumpia PO, Kronenberger EB, Hoi XP, Su B, Chi X, Bui VL et al (2020) Toll-like receptors induce signal-specific reprogramming of the macrophage lipidome. *Cell Metab* 32: 128–143
- Hudson JB (1988) Further studies on the mechanism of centrifugal enhancement of cytomegalovirus infectivity. *J Virol Methods* 19: 97–108
- Isaacs A, Lindenmann J (1957) Virus interference. I. The interferon. *Proc Royal Soc Lond* 147: 258–267
- Ivashkiv LB, Donlin LT (2014) Regulation of type I interferon responses. *Nat Rev Immunol* 14: 36–49
- Iyer SS, He Q, Janczy JR, Elliott EI, Zhong Z, Olivier AK, Sadler JJ, Knepper-Adrian V, Han R, Qiao L et al (2013) Mitochondrial cardiolipin is required for Nlrp3 inflammasome activation. *Immunity* 39: 311–323
- Janeway CA Jr, Medzhitov R (2002) Innate immune recognition. *Annu Rev Immunol* 20: 197–216
- King MP, Attardi G (1989) Human cells lacking mtDNA: repopulation with exogenous mitochondria by complementation. *Science* 246: 500–503
- Konno Y, Kimura I, Uriu K, Fukushi M, Irie T, Koyanagi Y, Sauter D, Gifford RJ, USFQ-COVID19 Consortium, Nakagawa S et al (2020) SARS-CoV-2 ORF3b is a potent interferon antagonist whose activity is increased by a naturally occurring elongation variant. *Cell Rep* 32: 108185
- Lee AJ, Ashkar AA (2018) The dual nature of type I and type II interferons. *Front Immunol* 9: 2061
- Lei X, Dong X, Ma R, Wang W, Xiao X, Tian Z, Wang C, Wang Y, Li L, Ren L et al (2020) Activation and evasion of type I interferon responses by SARS-CoV-2. *Nat Commun* 11: 3810
- Levy DE, Kessler DS, Pine R, Reich N, Darnell JE Jr (1988) Interferon-induced nuclear factors that bind a shared promoter element correlate with positive and negative transcriptional control. *Genes Dev* 2: 383–393
- Lio CW, McDonald B, Takahashi M, Dhanwani R, Sharma N, Huang J, Pham E, Benedict CA, Sharma S (2016) cGAS-STING signaling regulates initial innate control of cytomegalovirus infection. *J Virol* 90: 7789–7797
- Lordén G, Sanjuán-García I, de Pablo N, Meana C, Alvarez-Miguel I, Pérez-García MT, Pelegrín P, Balsinde J, Balboa MA (2017) Lipin-2 regulates NLRP3 inflammasome by affecting P2X7 receptor activation. *J Exp Med* 214: 511–528
- Low H, Mukhamedova N, Cui HL, McSharry BP, Avdic S, Hoang A, Ditiatkovski M, Liu Y, Fu Y, Meikle PJ et al (2016) Cytomegalovirus restructures lipid rafts via a US28/CDC42-mediated pathway, enhancing cholesterol efflux from host cells. *Cell Rep* 16: 186–200
- Majeed HA, Kalaawi M, Mohanty D, Teebi AS, Tunjekar MF, al-Gharbawy F, Majeed SA, al-Gazzar AH (1989) Congenital dyserythropoietic anemia and chronic recurrent multifocal osteomyelitis in three related children and the association with Sweet syndrome in two siblings. *J Pediatr* 115: 730–734
- Man SM, Karki R, Kanneganti TD (2017) Molecular mechanisms and functions of pyroptosis, inflammatory caspases and inflammasomes in infectious diseases. *Immunol Rev* 277: 61–75
- Martinon F, Burns K, Tschopp J (2002) The inflammasome: a molecular platform triggering activation of inflammatory caspases and processing of proIL-beta. *Mol Cell* 10: 417–426
- Masood KI, Yameen M, Ashraf J, Shahid S, Mahmood SF, Nasir A, Nasir N, Jamil B, Ghanchi NK, Khanum I et al (2021a) Upregulated type I interferon responses in asymptomatic COVID-19 infection are associated with improved clinical outcome. *Sci Rep* 11: 22958
- Masood KI, Yameen M, Nasir A, Shahid S, Hasan Z (2021b) Gene Expression Omnibus GSE177477. (<https://www.ncbi.nlm.nih.gov/geo/query/acc.cgi?acc=GSE177477>). [DATASET]
- Masters SL, Simon A, Aksentjevich I, Kastner DL (2009) Horror autoinflammaticus: the molecular pathophysiology of autoinflammatory disease. *Annu Rev Immunol* 27: 621–668
- Mathys S, Schroeder T, Ellwart J, Koszinowski UH, Messerle M, Just U (2003) Dendritic cells under influence of mouse cytomegalovirus have a physiologic dual role: to initiate and to restrict T cell activation. *J Infect Dis* 187: 988–999
- McDermott MF, Aksentjevich I, Galon J, McDermott EM, Ogunkolade BW, Centola M, Mansfield E, Gadina M, Karenko L, Pettersson T et al (1999) Germline mutations in the extracellular domains of the 55 kDa TNF receptor, TNFR1, define a family of dominantly inherited autoinflammatory syndromes. *Cell* 97: 133–144
- Meana C, Peña L, Lordén G, Esquinas E, Guijas C, Valdearcos M, Balsinde J, Balboa MA (2014) Lipin-1 integrates lipid synthesis with proinflammatory responses during TLR activation in macrophages. *J Immunol* 193: 4614–4622
- Miorin L, Kehrer T, Sanchez-Aparicio MT, Zhang K, Cohen P, Patel RS, Cupic A, Makio T, Mei M, Moreno E et al (2020) SARS-CoV-2 Orf6 hijacks Nup98 to block STAT nuclear import and antagonize interferon signaling. *Proc Natl Acad Sci USA* 117: 28344–28354
- Nakahira K, Haspel JA, Rathinam VA, Lee SJ, Dolinay T, Lam HC, Englert JA, Rabinovitch M, Cernadas M, Kim HP et al (2011) Autophagy proteins regulate innate immune responses by inhibiting the release of mitochondrial DNA mediated by the NALP3 inflammasome. *Nat Immunol* 12: 222–230
- Nelson EA, Walker SR, Kepich A, Gashin LB, Hideshima T, Ikeda H, Chauhan D, Anderson KC, Frank DA (2008) Nifuroxazide inhibits survival of multiple myeloma cells by directly inhibiting STAT3. *Blood* 112: 5095–5102
- Ng SL, Friedman BA, Schmid S, Gertz J, Myers RM, Tenover BR, Maniatis T (2011a) I $\kappa$ B kinase epsilon (IKK $\epsilon$ ) regulates the balance between type I and type II interferon responses. *Proc Natl Acad Sci USA* 108: 21170–21175
- Ng SL, Friedman BA, Schmid S, Gertz J, Myers RM, Tenover BR, Maniatis T (2011b) Gene Expression Omnibus GSE33913. (<https://www.ncbi.nlm.nih.gov/geo/query/acc.cgi?acc=GSE33913>) [DATASET]

- Péterfy M, Phan J, Xu P, Reue K (2001) Lipodystrophy in the *fld* mouse results from mutation of a new gene encoding a nuclear protein, lipin. *Nat Genet* 27: 121–124
- Pindado J, Balsinde J, Balboa MA (2007) TLR-3-dependent induction of nitric oxide synthase in macrophages via a cytosolic phospholipase A<sub>2</sub>/cyclooxygenase-2 pathway. *J Immunol* 179: 4821–4828
- Raza S, Barnett MW, Barnett-Itzhaki Z, Amit I, Hume DA, Freeman TC (2014a) Analysis of the transcriptional networks underpinning the activation of murine macrophages by inflammatory mediators. *J Leukoc Biol* 96: 167–183
- Raza S, Freeman TC, Hume DA (2014b) Gene Expression Omnibus GSE44292. (<https://www.ncbi.nlm.nih.gov/geo/query/acc.cgi?acc=GSE44292>) [DATASET]
- Robertson KA, Ghazal P (2016) Gene expression Omnibus GSE63290. (<https://www.ncbi.nlm.nih.gov/geo/query/acc.cgi?acc=GSE63290>) [DATASET]
- Robertson KA, Hsieh WY, Forster T, Blanc M, Lu H, Crick PJ, Yutuc E, Watterson S, Martin K, Griffiths SJ et al (2016) An interferon regulated microRNA provides broad cell-intrinsic antiviral immunity through multihit host-directed targeting of the sterol pathway. *PLoS Biol* 14: e1002364
- Rottenberg H, Hoek JB (2017) The path from mitochondrial ROS to aging runs through the mitochondrial permeability transition pore. *Aging Cell* 16: 943–955
- Rovas A, Osiaevi I, Buscher K, Sackarnd J, Tepaspe PR, Fobker M, Kühn J, Braune S, Göbel U, Thölking G et al (2021) Microvascular dysfunction in COVID-19: the MYSTIC study. *Angiogenesis* 24: 145–157
- Rubio JM, Rodríguez JP, Gil-de-Gómez L, Guijas C, Balboa MA, Balsinde J (2015) Group V secreted phospholipase A<sub>2</sub> is up-regulated by interleukin-4 in human macrophages and mediates phagocytosis via hydrolysis of ethanolamine phospholipids. *J Immunol* 194: 3327–3339
- Ruipérez V, Astudillo AM, Balboa MA, Balsinde J (2009) Coordinate regulation of Toll-like receptor-mediated arachidonic acid mobilization in macrophages by group IVA and group V phospholipase A<sub>2</sub>s. *J Immunol* 182: 3877–3883
- Schmittgen TD, Livak KJ (2008) Analyzing real-time PCR data by the comparative C(T) method. *Nat Protoc* 3: 1101–1108
- Schneider WM, Chevillotte MD, Rice CM (2014) Interferon-stimulated genes: a complex web of host defenses. *Annu Rev Immunol* 32: 513–545
- Schoggins JW, Wilson SJ, Panis M, Murphy MY, Jones CT, Bieniasz P, Rice CM (2011) A diverse range of gene products are effectors of the type I interferon antiviral response. *Nature* 472: 481–485
- Semper C, Leitner NR, Lassnig C, Parrini M, Mahlaköiv T, Rammerstorfer M, Lorenz K, Rigler D, Müller S, Kolbe T et al (2014a) STAT1β is not dominant negative and is capable of contributing to gamma interferon-dependent innate immunity. *Mol Cell Biol* 34: 2235–2248
- Semper C, Leitner NR, Lassnig C, Parrini M, Mahlaköiv T, Rammerstorfer M, Lorenz K, Rigler D, Müller S, Kolbe T et al (2014b) Gene Expression Omnibus GSE48970. (<https://www.ncbi.nlm.nih.gov/geo/query/acc.cgi?acc=GSE48970>) [DATASET]
- Seo J-Y, Yaneva R, Hinson ER, Cresswell P (2011) Human cytomegalovirus directly induces the antiviral protein viperin to enhance infectivity. *Science* 332: 1093–1097
- Sinzger C, Hahn G, Digel M, Katona R, Sampaio KL, Messerle M, Hengel H, Koszinowski U, Brune W, Adler B (2008) Cloning and sequencing of a highly productive, endotheliotropic virus strain derived from human Cytomegalovirus TB40/E. *J Gen Virol* 89: 359–368
- Smith GL, Talbot-Cooper C, Lu Y (2018) How does Vaccinia virus interfere with interferon? *Adu Virus Res* 100: 355–378
- Sodeifian F, Nikfarjam M, Kian N, Mohamed K, Rezaei N (2022) The role of type I interferon in the treatment of COVID-19. *J Med Virol* 94: 63–81
- Stark GR, Darnell JE Jr (2012) The JAK-STAT pathway at twenty. *Immunity* 36: 503–514
- Tartey S, Kanneganti TD (2020) Inflammasomes in the pathophysiology of autoinflammatory syndromes. *J Leukoc Biol* 107: 379–391
- Thoms M, Buschauer R, Ameismeier M, Koepke L, Denk T, Hirschenberger M, Kratzat H, Hayn M, Mackens-Kiani T, Cheng J et al (2020) Structural basis for translational shutdown and immune evasion by the Nsp1 protein of SARS-CoV-2. *Science* 369: 1249–1255
- Toshchakov V, Jones BW, Perera PY, Thomas K, Cody MJ, Zhang S, Williams BR, Major J, Hamilton TA, Fenton MJ et al (2002) TLR4, but not TLR2, mediates IFN-β-induced STAT1α/β-dependent gene expression in macrophages. *Nat Immunol* 3: 392–398
- Valdearcos M, Esquinas E, Meana C, Gil-de-Gómez L, Guijas C, Balsinde J, Balboa MA (2011) Subcellular localization and role of lipin-1 in human macrophages. *J Immunol* 186: 6004–6013
- Valdearcos M, Esquinas E, Meana C, Peña L, Gil-de-Gómez L, Balsinde J, Balboa MA (2012) Lipin-2 reduces proinflammatory signaling induced by saturated fatty acids in macrophages. *J Biol Chem* 287: 10894–10904
- Vinh DC, Abel L, Bastard P, Cheng MP, Condino-Neto A, Gregersen PK, Haerynck F, Cicalese MP, Hagin D, Soler-Palacín P et al (2021) Harnessing type I IFN immunity against SARS-CoV-2 with early administration of IFN-β. *J Clin Immunol* 41: 1425–1442
- Wagner M, Jonjic S, Koszinowski UH, Messerle M (1999) Systematic excision of vector sequences from the BAC-cloned herpesvirus genome during virus reconstitution. *J Virol* 73: 7056–7060
- Watahiki A, Shimizu K, Hoshikawa S, Chiba M, Kitamura H, Egusa H, Fukumoto S, Inuzuka H (2020) Lipin-2 degradation elicits a proinflammatory gene signature in macrophages. *Biochem Biophys Res Commun* 524: 477–483
- West AP, Khoury-Hanold W, Staron M, Tal MC, Pineda CM, Lang SM, Bestwick M, Duguay BA, Raimundo N, MacDuff DA et al (2015) Mitochondrial DNA stress primes the antiviral innate immune response. *Nature* 520: 553–557
- Winquist RJ, Gribkoff VK (2020) Targeting putative components of the mitochondrial permeability transition pore for novel therapeutics. *Biochem Pharmacol* 177: 113995
- Xia H, Cao Z, Xie X, Zhang X, Chen JY, Wang H, Menachery VD, Rajsbaum R, Shi PY (2020) Evasion of type I interferon by SARS-CoV-2. *Cell Rep* 33: 108234
- Xu D, Biswal M, Neal A, Hai R (2021) Review Devil's tools: SARS-CoV-2 antagonists against innate immunity. *Curr Res Virol Sci* 2: 100013
- Zhang P, Reue K (2017) Lipin proteins and glycerolipid metabolism: roles at the ER membrane and beyond. *Biochim Biophys Acta* 1859: 1583–1595
- Zhang Y, Liu T, Meyer CA, Eeckhoutte J, Johnson DS, Bernstein BE, Nusbaum C, Myers RM, Brown M, Li W et al (2008) Model-based analysis of ChIP-Seq (MACS). *Genome Biol* 9: R137
- Zhang Q, Bastard P, Bolze A, Jouanguy E, Zhang SY, Human Genetic Effort COVID, Cobat A, Notarangelo LD, Su HC, Abel L et al (2020a) Life-threatening COVID-19: defective interferons unleash excessive inflammation. *Med* 1: 14–20
- Zhang Q, Bastard P, Liu Z, Le Pen J, Moncada-Velez M, Chen J, Ogishi M, Sabli IKD, Hodeib S, Korol C et al (2020b) Inborn errors of type I IFN immunity in patients with life-threatening COVID-19. *Science* 370: eabd4570
- Zhang Q, Matuozzo D, Le Pen J, Lee D, Moens L, Asano T, Bohlen J, Liu Z, Moncada-Velez M, Kendir-Demirkol Y et al (2022) Recessive inborn errors

of type I IFN immunity in children with COVID-19 pneumonia. *J Exp Med* 219: e20220131

Zhong Z, Liang S, Sanchez-Lopez E, He F, Shalpour S, Lin XJ, Wong J, Ding S, Seki E, Schnabl B *et al* (2018) New mitochondrial DNA synthesis enables NLRP3 inflammasome activation. *Nature* 560: 198–203

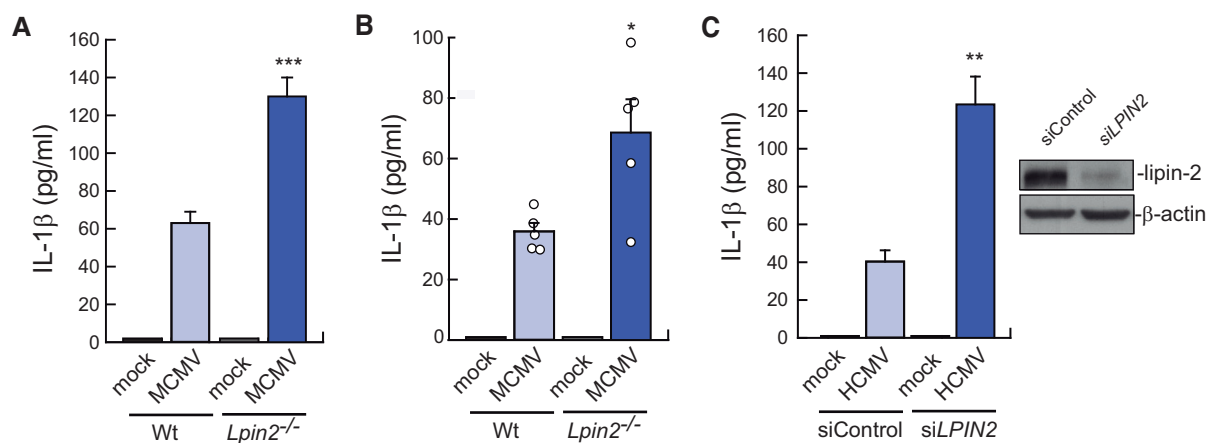
Zhou R, Yazdi AS, Menu P, Tschopp J (2011) A role for mitochondria in NLRP3 inflammasome activation. *Nature* 469: 221–225

Zhou P, Yang XL, Wang XG, Hu B, Zhang L, Zhang W, Si HR, Zhu Y, Li B, Huang CL *et al* (2020) A pneumonia outbreak associated with a new coronavirus of probable bat origin. *Nature* 579: 270–273



**License:** This is an open access article under the terms of the [Creative Commons Attribution-NonCommercial-NoDerivs](https://creativecommons.org/licenses/by-nc-nd/4.0/) License, which permits use and distribution in any medium, provided the original work is properly cited, the use is non-commercial and no modifications or adaptations are made.

## Expanded View Figures



**Figure EV1. Lipin-2 effects on IL-1β production during cytomegalovirus infection.**

- A LPS-primed BMDMs from Wt or *Lpin2*<sup>-/-</sup> animals were mock infected or infected with MCMV (MOI = 2). IL-1β levels were measured in cell supernatants using a specific ELISA after 36 h of infection.
- B Wt (*n* = 5) and *Lpin2*<sup>-/-</sup> (*n* = 5) animals were intraperitoneally injected with MCMV ( $3.5 \times 10^6$  PFU per mouse) and IL-1β levels were evaluated in serum using specific ELISAs after 36 h of infection.
- C LPS-primed primary human macrophages, nucleofected with control siRNAs (siControl) or against *LPIN2* (siLPIN2), were mock infected or infected with HCMV (MOI = 5) for 36 h. IL-1β levels in cell supernatants were measured in cell supernatants using a specific ELISA. Right insert: lipin-2 expression in silenced cells by immunoblot.

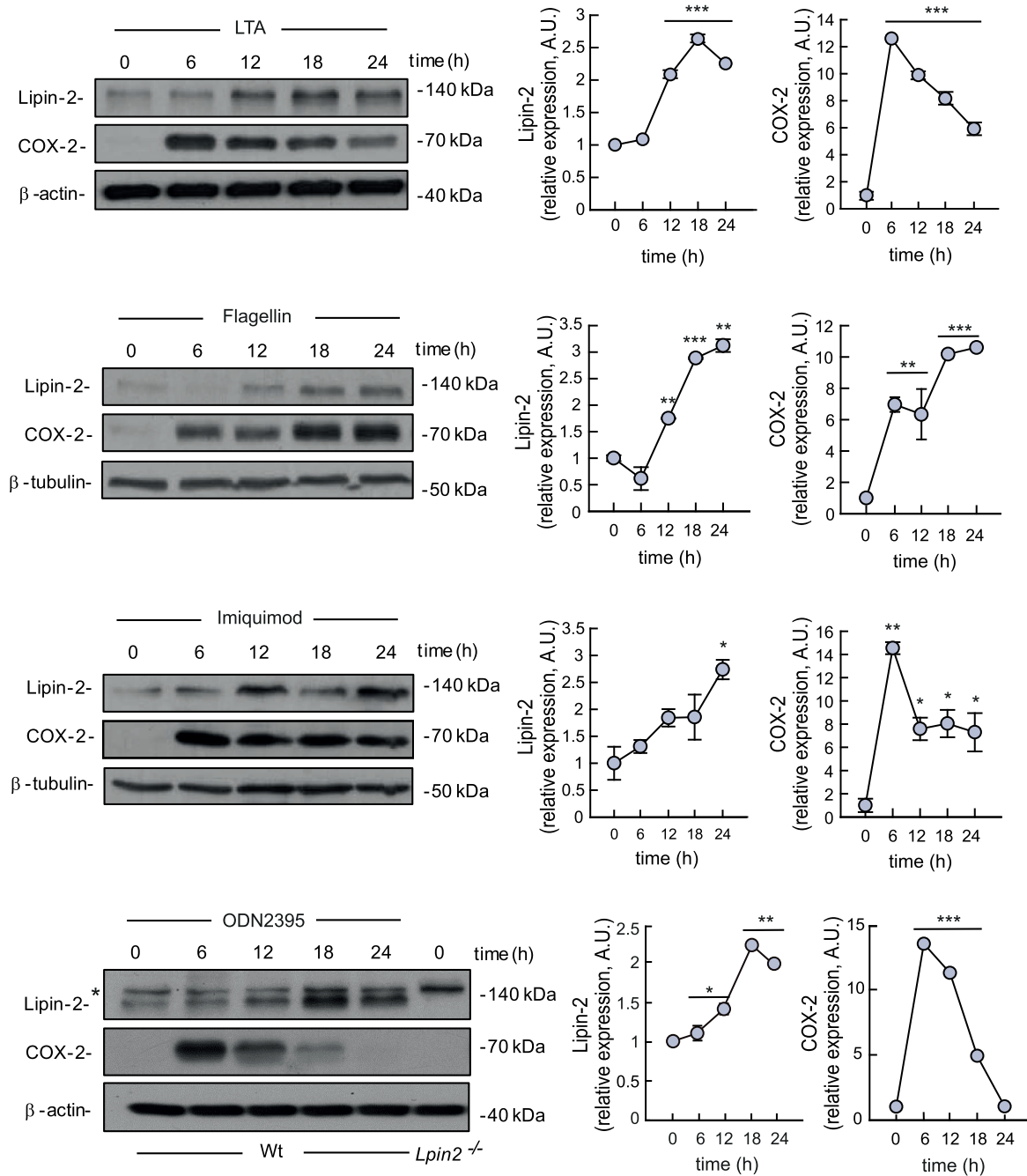
Data information: Data shown are from biological triplicate samples and are expressed as means  $\pm$  SEM. \**P* < 0.05; \*\**P* < 0.01, \*\*\**P* < 0.001, by Student's *t*-test.



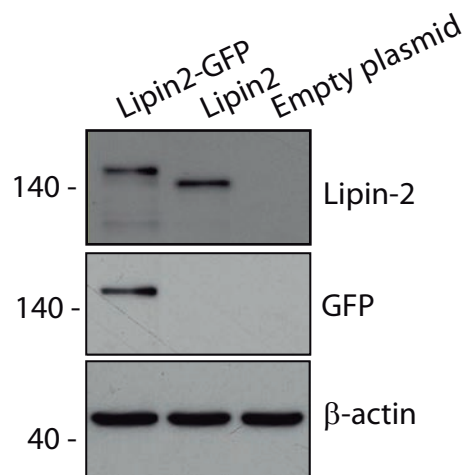
# Appendix

## Table of contents

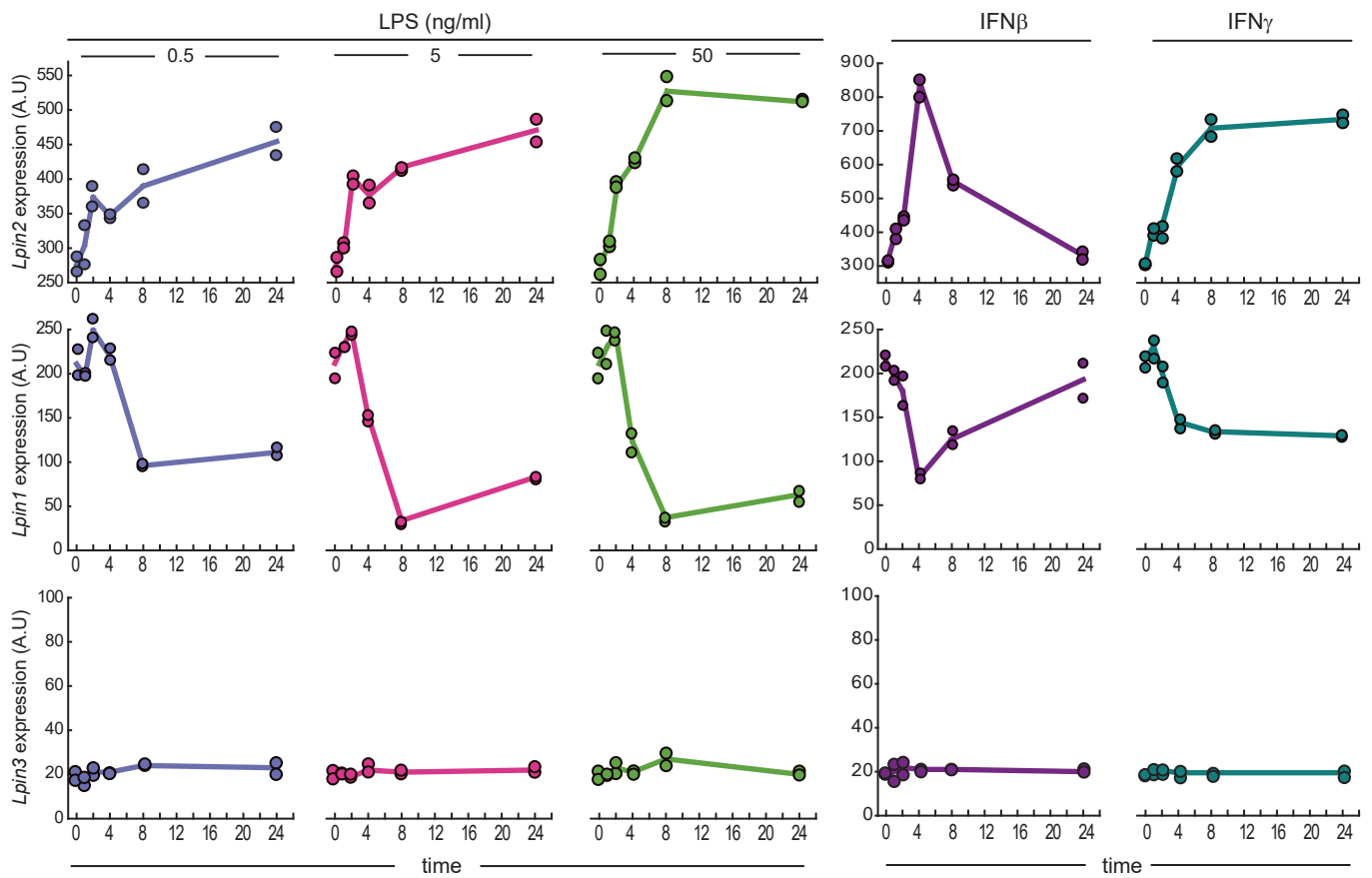
Appendix Figure S1.....	2
Appendix Figure S2.....	3
Appendix Figure S3.....	4
Appendix Figure S4.....	5
Appendix Figure S5.....	6
Appendix Figure S6.....	7
Appendix Figure S7.....	8
Appendix Figure S8.....	9



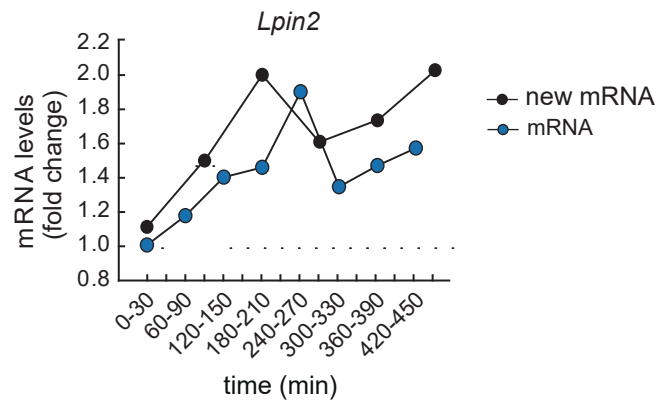
**Appendix Figure S1.** (continuation of Fig 1). *Effect of TLR agonists on lipin-2 expression.* BMDMs were treated with 1  $\mu$ g/ml LTA (TLR2), 50 ng/ml Flagellin (TLR5), 5  $\mu$ g/ml Imiquimod (TLR7) or 1  $\mu$ M ODN 2395 (TLR9) for the indicated periods of time. Cells lysates were analyzed by immunoblot using specific antibodies against lipin-2, COX-2, and  $\beta$ -actin or tubulin as loading controls. Quantifications of the bands from technical replicates are shown on the right. Shown are representative experiments of three ones. \*,  $P < 0.05$ , \*\*  $P < 0.01$ , \*\*\*  $< 0.001$ , by Student's t test.



**Appendix Figure S2.** *Overexpression of lipin-2 in HEK-239 cells.* HEK-239 cells were transfected with 2  $\mu$ g of the plasmid mlipin-2-EGFP (Valdearcos et al., 2012, J. Biol. Chem. 287: 10894-10904) containing the murine sequence of lipin-2 fused with EGFP, a plasmid containing only the lipin-2 sequence or with an empty plasmid. Lysates were analyzed by immuno-blot using antibodies against lipin-2, GFP and  $\beta$ -actin.

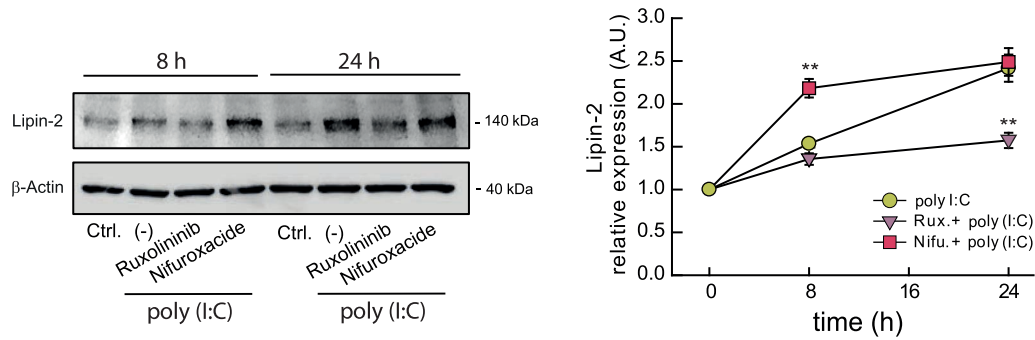


**Appendix Figure S3.** *Lpin* mRNA expression levels in activated BMDMs. BMDMs were treated with the indicated doses of LPS (left panels), or 10 U/ml of IFN $\beta$  or IFN $\gamma$  (right panels). Duplicate samples were collected at 0, 1, 2, 4, 8 and 24 h. mRNA levels for the indicated lipins were analyzed using Affymetrix Mouse Gene 1.1ST Array (GSE44292) (Raza et al., 2014, *J. Leukoc. Biol.* 96:167-183).



**Appendix Figure S4.** New synthesis of *Lpin2* mRNA induced by IFN- $\gamma$ . BMDMs were treated or not with 100 U/ml IFN- $\gamma$  at different time points and newly transcribed mRNA and total RNA was analyzed as described elsewhere (Dölken L et al., 2008, RNA, 14:1959-1972). Fold change of newly transcribed and total levels of *Lpin2* mRNA from stimulated cells is represented.





**Appendix Figure S5.** *Lipin-2* expression in cells treated with *poly(I:C)*. BMDMs were left untreated (Ctrl.) or stimulated with 25 mg/ml *poly(I:C)* in the presence or absence of 5 mM Ruxolitinib or 10 mM Nifuroxamide for the indicated periods of time. Protein was analyzed by Immunoblot using specific antibodies against lipin-2 or  $\beta$ -actin (loading control). Quantifications of the bands are shown on the right. Shown is a representative experiment of three ones (three biological samples). \*\*,  $P < 0.01$ , by Student's t test.

**Peak 1:** 71527697-71528898

CAGGAGTGTAGCTGGATAGGAGAAAGAACTTCTAGAGTTTTGACTGTGGTTGGCGTCAATTAATTGCATACTT  
AGAATTACTTGTAGACAAGATCACGAATGTTCCCTAAAACAAAGAACTAAACACAAGCCAGTTTTCTTCATTA  
TCATCACATCCTTAGAGATGTATTGAAATGTCATGCTATGTCACCTAAAAATTTACACTTTTGTGAGTTAATT  
AGAAATAAAGTATATCTTCCCCCAAACAGCTTTCAGAGTCCAGGAGTCCAGGATAGCTTTCAGCACCAC  
CAGTTACAAGCCGTGGGAACCTTACTTGAGTCACTCCTGTCTCCGTTGAATATAATTACAAAACGAGCTGGGTC  
TACTGTGGCGGTGCAGGAAACCCAGGCTGTCATCTGACCCAGGGAACATCAAAGCCAGGAACAGAAAAGCTGC  
TTTTCTAAAGTTTTCGTTCCCTACCTCACCTGTCTCAGAGCTGCCAGGCAGGAGGGTGTAGGAGCTTTCCCTC  
CTGACTCCAGAGAAAGCTCTCTTTCAGGAAATGAAAGACACATTTTTCTCCCTCTTGACTTGGGTGCTTTGGTGA  
TTTTAGAGTTTTGGGAAATAACAGACAGGAAGGAAACATCTTGCAGGCAACTTCTGCTTCTCATCTCCCCAGCA  
GACTTCCCCAAGACAAGTGGCATGCCTGCTGAATCTTGTAAAGAGGAGCGTGCAGGGAGAAATGTGGAAGCT  
AATATTTAAAAAGTTATCACACTGCAGAAGGACCGGCTGACGCACATAGAACGGGAGAGACAACCTGGAGCAAA  
AGGGGGCACTGCTTCTTGGGAGGTCAGTCTTTGTATTGAAGGCAAAGGACTGGCAAGGACAGATCTGCCAAA  
CGAGGGTGGGTGGTTAGTATTACTGGCTGGAGGGATGGGAAGAAAGCTCTTTTGCCTTCTGGACTTTCAGAG  
AGATGGAGAGATTTACTGCAACTAGGGAGAGGTCGCAAATTTGGACAACCTGAAGAGGATATGACTTGTGCCTGT  
GGTAGCCATTCTTCAGAGAACTTTAGACAGTAGACATGCTGAGGTAGGGAGGGTGGACATGTGATGACAGTAC  
CGGAATTGAGACTCTTCCCTAGGTTTCCGACAAAGATGACTAAATGGTTGGTAGTGCCATTAGCTGGGATATG  
AGATTC

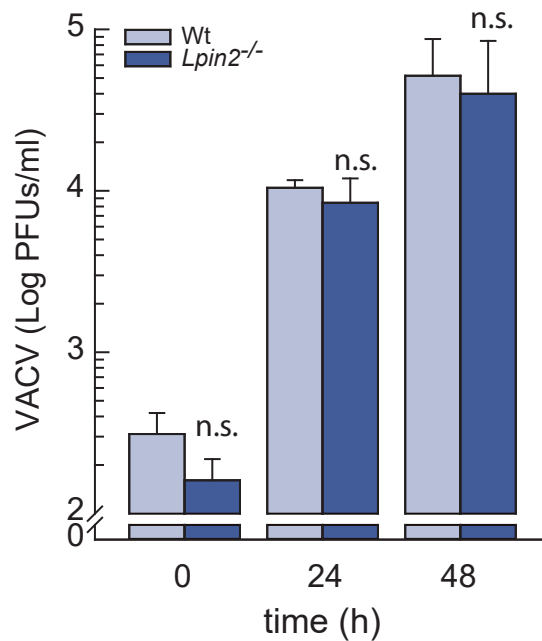
**Peak 2:** 71539873-71540425

CTAATTGTGCAAAATAACTGACTTTATCGAGGCATTTTTCTCATGATACTTTTGGCACATGGTTCACTCGGTTG  
TCTCTTGGAGACCTGCATGCCTGCCCGCTTGGCTATGTCTGATACTAGATGAGGGTGTGTGTTAAAGCATACC  
TGTTTTGGAAGACTGCGAGCTAAGGGCGAGTCACGGGGCAAAGGGAGACCTGAAAGTAACTTGTAGTGCTGTG  
GGGGAAGTGAAGTACTGATCTCACGTATAAAATAAAGCAGGGTGTCTAAACGGAGGCCCTGAGGGTTAGGAA  
TGGGAGTCAGCTTAGAGAATTGAAAGTGAAAAGGCAAAGAAGTATCTTGGGGAGAGCTCCTGTGTTTATATTTT  
TAGTGTGTCAATGTTTACTTGAAGGATTTTTTTTTTTAATATTTCAAGGAAACCATTTTTGTGTGCTTGCATAG  
ATTTCTTCCCTTGACTCTTGCCTTCCCTAGCGACAATACGAGCAGTTTTTGTGCTGATAGTTGATAAAGTTAGG  
AGTGACTATTTTTGTGTGAATTCTAGTTCATGTTAATAAAA

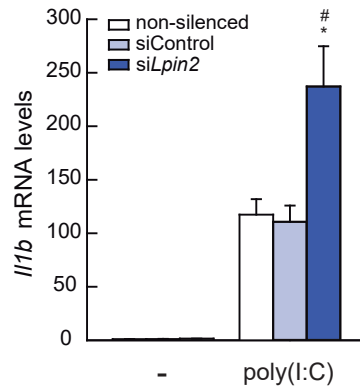
**Peak 3:** 71541311-71541719

AGGGGATTCCAGAGGCTCTTGGCATTGTTGTCTGTTAGGATTGTCATTGGTGGACCCTTCGGTCGTTCTGGTAT  
GGCCTTTCAAGGACTTCCATGGTTTTAGTTTTATTGTTATAGCTCTTGAGATGAGGACTGGGGGATGCCACTAT  
GTCCAAGACCTCACCAGCTTTTAGAGAAGTACTGAGTATTTCTGTGGGATGCCTCACTGTAAGTTTTCTTATT  
GCTTTCTCATGATAAGACTGGGTTATGACTAAGGAAGACCACAGAGGGTAAAGTACCTTGTGACTCATGGTGG  
TCATGGCCTTGATCAACAGCAGTTTTGAGGTTGTGTGTTTCAGATTTTTCTCTACTGACAACCTAATTTGTATT  
TTTTCTATGTATAAGAAGTTTGTAGGGGGGTCGTAAGGGGGG

**Appendix Figure S6.** *ISRE and GAS sequences present in Stat1 peaks in the Lpin2 gene.* DNA sequence motifs recognized by Stat1 in peaks 1, 2 and 3 called by MACS during Chip-Seq analysis were determined by the presence of ISRE (GAAANNGAAA, green) or GAS (TTCNNNGAA or TTCNNNGAA, grey) consensus motifs within a 100-bp region centered on the peak summit. Notice that in peak 2 a GAS consensus motif was also found at 128-bp from the center of the peak.



**Appendix Figure S7.** Infection of BMDMs with VACV is not affected by lipin-2 expression levels. BMDMs from Wt or Lpin2<sup>-/-</sup> animals were infected with VACV (MOI = 0.01, Western Reserve strain). Cells were harvested at the indicated time points and virus yields were determined by plaque assay in BSC40 cells. Results represent the mean ± SD of three independent experiments. *P* values were calculated by two-tailed t test assuming non-equal variance. No statistical differences (n.s.) were found between Wt and lipin-2 –deficient macrophages.



**Appendix Figure S8.** *Effect of lipin-2 on Il1b expression in RAW264.7 macrophages.* RAW264.7 macrophages were left untreated (non-silenced), or silenced with control siRNAs (siControl) or against *Lpin2* (siLpin2). After 48 h, cells were left untreated (-) or activated with 25  $\mu\text{g/ml}$  poly(I:C). *Il1b* mRNA levels were analyzed by qPCR, using *Gapdh* as reference. Data from triplicate biological samples are represented as mean  $\pm$  SE. \*,  $P < 0.05$ , #,  $P < 0.05$ , by Student's t test. \*, siLpin2 vs siControl. #, siLpin2 vs non-silenced cells.